MRAP2 modifies the signaling and oligomerization state of the melanocortin-4 receptor

Iqra Sohail[1,6]*, Suli-Anne Laurin[2]*, Gunnar Kleinau[3], Vidicha Chunilal[4], Andrew Morton[5], Zeynep Cansu Uretmen Kagiali[6], Javier A. Tello[7], Martin J. Lohse[1,8,9], Patrick Scheerer[3], Michel Bouvier[2#], Peter McCormick[4,10#], Paolo Annibale[1,5#], Heike Biebermann[6#]

Affiliations

1 Max-Delbrück-Center for Molecular Medicine, Berlin

2 Institute for Research in Immunology and Cancer, Department of Biochemistry and Molecular Medicine, Université de Montréal

3 Charité Universitätsmedizin Berlin, corporate member of Freie Universität Berlin and Humboldt-Universität zu Berlin, Institute of Medical Physics and Biophysics, Group Structural Biology of Cellular Signaling, Berlin

4 Centre for Endocrinology, William Harvey Research Institute Queen Mary University of London

5 School of Physics and Astronomy, University of St Andrews

6 Charité Universitätsmedizin Berlin, corporate member of Freie Universität Berlin and Humboldt-Universität zu Berlin, Institute for Experimental Paediatric Endocrinology

7 School of Medicine, University of St Andrews

8 ISAR Bioscience Institute, Planegg/Munich

9 Rudolf Boehm Institute for Pharmacology and Toxicology, University of Leipzig

10 Department of Pharmacology and Therapeutics, University of Liverpool and XJTLU-University of Liverpool Joint Centre for Pharmacology and Therapeutics.

* equal contribution

#michel.bouvier@umontreal.ca, peter.mccormick@liverpool.ac.uk, pa53@st-andrews.ac.uk, heike.biebermann@charite.de

ABSTRACT

The melanocortin-4 receptor (MC4R) is a G protein-coupled receptor (GPCR) and a key regulator of appetite and metabolism. It can interact with the melanocortin-receptor accessory protein 2 (MRAP2), a single transmembrane helix protein known to interact with several different GPCRs. However, the consequences of this interaction are not completely understood. Here we report that co-expression of MRAP2 has multiple effects on the MC4R: it enhances G protein-mediated signaling and simultaneously impairs β-arrestin2 recruitment and, consequently, internalization. In addition, co-expression of MRAP2 leads to an increased number of monomers of MC4R by disrupting receptor oligomers. A structural homology model of the active state MC4R–MRAP2–Gs complex suggests interaction sites between MRAP2 and MC4R that are relevant for receptor activation. Taken together, our data indicate that MRAP2 is an accessory protein that interacts with and influences MC4R structure, biasing its signaling towards G protein-mediated effects.

INTRODUCTION

The melanocortin receptor accessory proteins (MRAPs), namely MRAP1 and MRAP2, are single helix membrane-spanning proteins that have been shown to interact with different G protein-coupled receptors (GPCRs)(Wang, Wang et al. 2022), such as the orexin 1 receptor (OXR1)(Rouault, Lee et al. 2017), prokineticin 1 receptor (PKR1)(Lattanzi, Casella et al. 2024) and ghrelin receptor (GHSR1a)(Asai, Ramachandrappa et al. 2013). It has been hypothesized that MRAPs act in a similar manner to another family of accessory proteins, called receptor activity-modifying proteins (RAMPs), which associate with numerous class B GPCRs(McLatchie, Fraser et al. 1998, Hay, Poyner et al. 2006, Mainland and Matsunami 2012, Klein, Matson et al. 2016, Serafin, Harris et al. 2020, Fan, Liu et al. 2022, Peters, Singh et al. 2022).

Both MRAP subtypes have been shown to interact with all five members of the melanocortin receptor (MCR) family(Chan, Webb et al. 2009). MRAP1 is mainly expressed in the adrenal gland and is essential for melanocortin-2 receptor (MC2R) trafficking to the cell surface as well as for adrenocorticotropin hormone (ACTH) binding. MC2R is essentially the sole and indispensable receptor mediating cortisol response to stress(Webb and Clark 2010). Mutations in MRAP1 as well as in MC2R result in familial glucocorticoid deficiency(Metherell, Chapple et al. 2005). Important evidence for this direct structural interaction between MRAPs and class A GPCRs was recently provided by the 3D structure of the active MC2R-G protein complex with ACTH and MRAP1, which was solved by cryo-electron microscopy (cryo-EM)(Luo, Feng et al. 2023). Functional studies indicated a reduction of MC4R signaling by MRAP1(Sebag and Hinkle 2007).

MRAP2 is predominantly expressed in tissues impacting metabolism and glucose homeostasis, including the central nervous system (CNS), the pancreas, the gut and adipose tissues(Hofland, Delhanty et al. 2012). Within the mouse CNS, especially in the hypothalamus and in the paraventricular nucleus (PVN), MRAP2 is co-expressed in some neurons together with the MC4R, where it has been proposed to be important for some MC4R functions(Asai, Ramachandrappa et al. 2013, Bruschetta, Kim et al. 2018, Liang, Li et al. 2018, Bernard, Ojeda Naharros et al. 2023). MRAP2 and MC4R messenger RNAs were both found in human PVN (The Human Protein Atlas) at a ratio around 3:1 (**Supplementary table 1**). The PVN is a hypothalamic region critical for energy homeostasis and the MC4R is a crucial player in energy metabolism (Kuhnen, Krude et al. 2019, Wade, Lam et al. 2021). For that reason, the MC4R is one of the prime targets for potential pharmacological regulation of appetite and body weight(Clement, Biebermann et al. 2018), as witnessed by more than 160 different pathogenic human variants causing obesity(Heyder, Kleinau et al. 2019).

In addition to rare human heterozygous *MRAP2* mutations that result in increased body weight, global and brain specific *Mrap2* deletion in mice leads to marked obesity(Asai, Ramachandrappa et al. 2013, Baron, Maillet et al. 2019). Moreover, a large-scale study in pigs identified *MRAP2* as a candidate gene associated with daily weight gain, supporting its importance for energy balance in different species(Cai, Christensen et al. 2022). This effect of body weight regulation is further underpinned by a previous study on the role of MRAP2 in zebrafish feeding and growth(Sebag, Zhang et al. 2013). In addition to its canonical Gs protein-dependent cell signaling, the MC4R activates the Gq/11 family signaling pathway, which is also involved in appetite regulation(Li, Shrestha et al. 2016). Agonist-stimulation further trigger β-arrestins recruitment to the receptor to terminate G-protein signaling and to initiate receptor endocytosis (Brouwers, de Oliveira et al. 2021).

Recent investigations on MRAP2 and MC4R pointed to an increase of signaling by co-expression of both proteins(Sebag, Zhang et al. 2013, Schonnop, Kleinau et al. 2016). It was hypothesized that the observed increase in Gs-mediated cAMP signaling could be related to MC4R homodimer separation(Schonnop, Kleinau et al. 2016). This scenario, however, has never been explored in detail experimentally, albeit MC4R homodimerization has been reported by us and others, both in

human MC4R and in orthologous forms such as *Xiphophorus* MC4R(Elsner, Tarnow et al. 2006, Piechowski, Rediger et al. 2013, Brouwers, de Oliveira et al. 2021, Reininghaus, Paisdzior et al. 2022).

Many questions regarding the mode of action and the resulting effects of the interaction between MRAP2 and MC4R are thus still unclear. In this study, we aimed to investigate the effect of MRAP2 on different MC4R signaling pathways and supramolecular organization, using a suite of fluorescence and bioluminescence resonance energy transfer (FRET and BRET)-based assays, single cell imaging and functional assays(Scarselli, Annibale et al. 2016). Collectively, our data point to an important role of MRAP2 in modulating the supramolecular organization state of MC4R, namely its increased monomerization, while directly impacting receptor signaling.

RESULTS

MRAP2 expression increases Gs-mediated cAMP accumulation in the basal and ligand-activated states of MC4R

To investigate the effect of MRAP2 action on MC4R signaling, we first examined the effect of MRAP2 expression on the MC4R-induced Gs activation in heterologously transfected HEK293 cells. Using the Epac-S^{H187} FRET biosensor(Klarenbeek, Goedhart et al. 2015), the increase in cAMP formation was determined as a reduction in FRET between a cyan fluorescent donor and a yellow fluorescent acceptor, and plotted as normalized FRET responses upon stimulation with the agonist α-MSH in the presence or absence of varying ratios of MC4R:MRAP2. In the literature, a wide range of transfection ratios of MRAPs:GPCRs (1:1 to 1:20) with highly variable outcomes are reported, without proper explanation for their selection. Our data show that upon co-expression of either the same DNA mass ratio of MC4R and MRAP2 (1:1, indicated as 1+1), or a fourfold excess of MRAP2 to MC4R (1:4 ratio, indicated as 1+4), there is a leftward shift of the average concentration response curves for a-MSH-stimulated cAMP production (**Figure 1A**), reflecting an increased potency of the agonist for the MC4R promoted cAMP production. Interestingly, both ratios lead to a similar shift in the EC_{50} obtained from fitting the concentration response curves using Hill's equation, namely from 4.5 nM to 1.3 nM, as seen in **Figure 1B**, suggesting a saturable effect.

We then determined basal (non-ligand stimulated) cAMP concentrations, in cells transfected with both MRAP2 and the MC4R, as opposed to cells transfected with the MC4R and mock DNA, to keep the DNA content stable. As shown in **Figure 1D**, a statistically significant increase in basal activity occurs when MRAP2 DNA is transfected in an excess of one or four parts to one part of MC4R DNA. Results are expressed as donor/FRET ratio, which increases proportionally to cAMP formation.

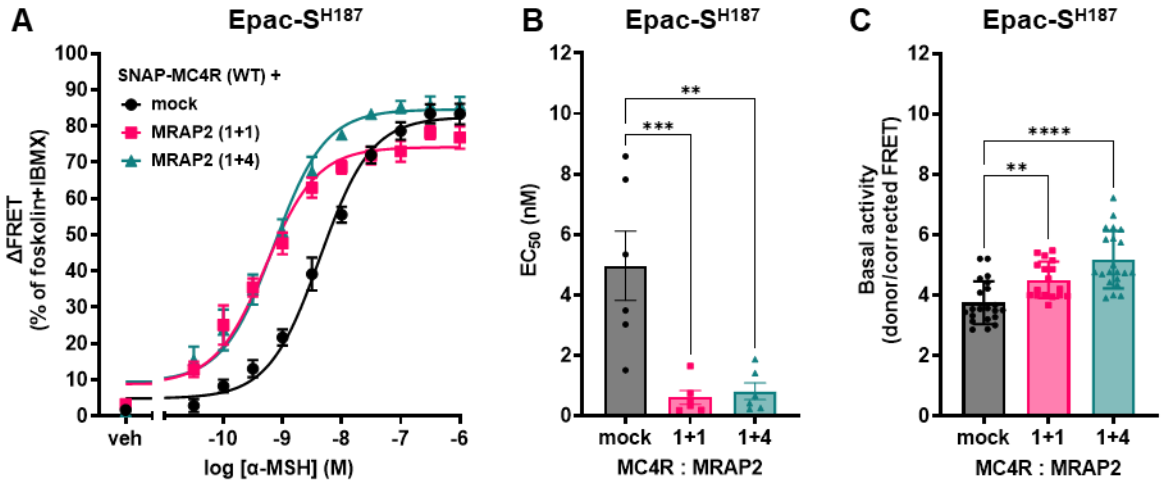

Figure 1: MRAP2 co-expression enhances cAMP signaling. (A) Average concentration-response curves of cAMP response upon MC4R stimulation with α-MSH, with and without different amounts of MRAP2 in transiently transfected HEK293 cells using the EpacS^{H187} biosensor. Data are normalized to forskolin response in the presence of the phosphodiesterase inhibitor IBMX (100%). MC4R is first expressed with an equivalent amount of pcDNA (mock). Plasmid DNA coding for MRAP2 is then co-expressed either in equivalent amounts (1+1) or with a 4-fold higher molar concentration with respect to the MC4R (1+4), always maintaining constant the total amount of DNA transfected. Mean and standard error of the mean (SEM) of six independent experiments (with three technical replicates each) are shown. **(B)** EC_{50} values obtained using the Epac-S^{H187} FRET biosensor. Points represent average EC_{50} across the six independent experiments, and mean and SEM are indicated. **(C)** Basal cAMP values (as assessed by FRET ratio) in the presence or absence of MRAP2 measured using the Epac-S^{H187} FRET biosensor in cells transfected different amounts of MRAP2 relative to the MC4R. Points represent the technical replicates across the six independent experiments, and mean and SD are indicated. One-way ANOVA as statistical test was performed with Dunnett's multiple comparisons post-hoc test.

To confirm whether the observations reported in **Figure 1A-C** can be ascribed to enhanced recruitment of the stimulatory heterotrimeric Gs protein at the agonist-bound MC4R, we exploited the nanobody 35 (Nb35), which recognizes the active conformation of $G\alpha_s$, and the miniGs, which binds the active conformation of Gs-coupled GPCR.

In our first assay, a fluorescently labeled Nb35 (Nb35-eYFP), which is known to bind with high affinity the active conformation of the $G\alpha_s$ subunit(Rasmussen, DeVree et al. 2011, Heyder, Kleinau et al. 2021), was transfected in HEK293 cells co-expressing SNAP-MC4R (**Figure 2A**). The addition of an N-terminal SNAP-tag does not affect MC4R downstream signaling (**Supplementary Figure 1**). Total internal fluorescence microscopy (TIRF) was then used to monitor the nanobody recruitment at the plasma membrane of MC4R-expressing cells upon stimulation with 1 µM of NDP-α-MSH. This agonist was employed to maximize the signal-to-noise ratio in these assays, since it is 30 times more potent than α-MSH(Sawyer, Sanfilippo et al. 1980). Cells were co-transfected with a plasmid coding for $G\alpha_s$ protein to ensure sufficient $G\alpha_s$ in the system to allow detection of the 1:1 stoichiometric recruitment of Nb35 to the receptors. Expression levels of $G\alpha_s$ were also confirmed to be stable in the presence or absence of MRAP2 with a fluorescently tagged version of $G\alpha_s$ (**Supplementary Figure 3**). **Figure 2A** illustrates the enhancement of Nb35 fluorescence (green) at the plasma membrane of SNAP-MC4R-expressing cells (gray) upon agonist addition, in the presence or absence of MRAP2. **Figure 2B** illustrates the kinetics of Nb35 recruitment to the membrane in both cases. Notably, MRAP2 significantly increased the kinetics of the nanobody recruitment, suggesting that $G\alpha_s$ recruitment to the receptor and its activation are indeed favored by the action of MRAP2.

These results are mirrored when measuring at ligand binding. Using a single cell-based fluorescence assay in conjunction with a fluorescently tagged NDP-α-MSH, we could observe that cells transfected with MRAP2 (1+4) bind significantly more ligand than the mock transfected counterparts (**Supplementary Figure 4A**) and that the number of NDP-α-MSH molecules bound, normalized by the number of receptors expressed, increases as a function of the expression level of MRAP2 in transiently transfected cells (**Supplementary Figure 4B,C**)

In the second assay, MC4R activation at the plasma membrane was confirmed by the increase in the BRET signal between Rluc8-miniGs, which recognizes the active form of $G\alpha_s$-coupled GPCR such as MC4R, and a *Renilla* green fluorescent protein (rGFP) targeted to the plasma membrane with the CAAX box of KRas(Wright, Motso et al. 2023). The half log-unit leftward shift of the concentration-response curve upon equivalent transfection of MC4R and MRAP2 (1+1) relative to the control mock conditions (**Figure 2C**) confirms that MRAP2 expression favors $G\alpha_s$-coupling (**Figure 2D**). RAMP3, for which no prior indication of an interaction with MC4R has been reported, was used as a negative control, and it indeed showed no effect on miniGs recruitment. In side-by-side experiments, there is also no change in BRET upon stimulation of cells not transfected with MC4R, showing the response is indeed dependent on this receptor (**Supplementary Figure 5A**).

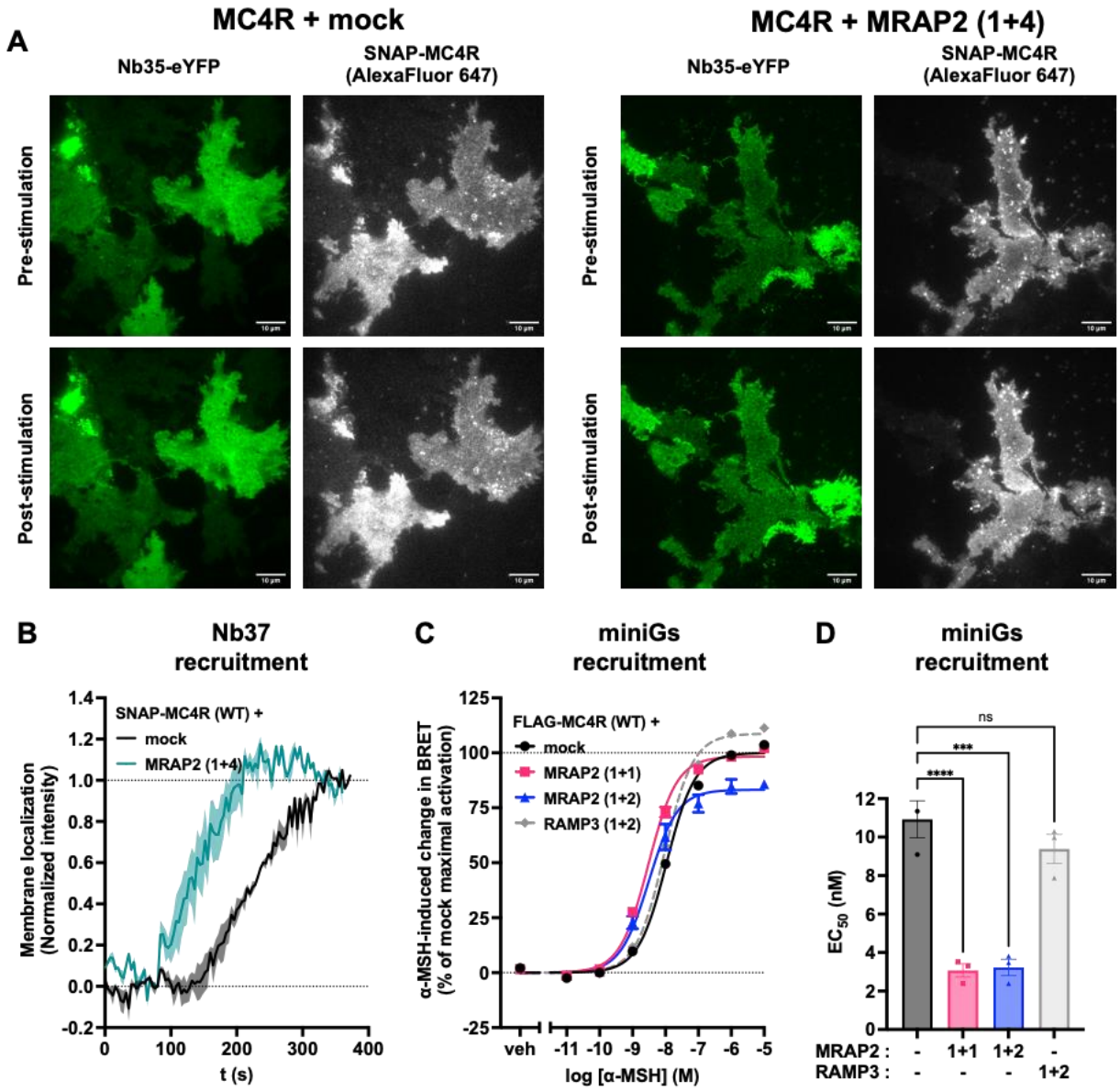

Figure 2: MRAP2 enhances Gα$_s$ activation by the MC4R. (A) Representative images from TIRF microscopy of the basolateral membrane of HEK293AD cells expressing SNAP-tagged MC4R labeled using Alexa Fluor 647 (gray) and Nb35-eYFP (green). Images were taken pre- (top) and 4 min post- (bottom) stimulation with 1 µM NDP-α-MSH for cells expressing SNAP-MC4R alone or with MRAP2 (at a ratio of 1:4) and indicate recruitment of Nb35 (green intensity). **(B)** Kinetics of recruitment of Nb35 to the SNAP-MC4R–Gs complex, without (black; 3 transfections, 51 single cells) and with MRAP2 (1+4) (turquoise; 3 transfections, 55 cells). Shown are the normalized mean fluorescence intensities recorded at the membrane in the eYFP channel; the shaded area represents SEM. **(C)** Average concentration-response curves of Rluc8-miniGs recruitment to the plasma membrane localization sensor rGFP-CAAX upon MC4R stimulation with α-MSH for 45 minutes, in the presence or absence of MRAP2 or RAMP3, at the indicated ratio with respect to MC4R, in transiently transfected HEK293-SL cells. Normalized data are expressed as mean ± SEM of three independent experiments. **(D)** EC_{50} values from the miniGs recruitment BRET experiments. Points represent average EC_{50} across the three independent experiments, and mean and SEM are indicated. Statistical analysis was performed using ordinary one-way ANOVA with Dunnett's multiple comparisons post-hoc test (*** = $p < 0.001$, **** = $p < 0.0001$).

MRAP2 increases MC4R-induced activation of Gq signaling pathway

Based on these observations, we further investigated the signal transduction by another G protein that has been shown to be engaged by MC4R, namely $G\alpha_q$, using two different sets of assays.

First, we exploited enhanced bystander BRET (ebBRET) between p63RhoGEF, an effector that selectively interacts with activated Gα subunits of the Gq/11 subfamily, and plasma membrane-targeted rGFP(Avet, Mancini et al. 2022). Upon co-expression with MRAP2, we observed a leftward shift of the concentration response curve upon stimulation with the agonist α-MSH, as well as an increase in the maximal response (E_{max}) (**Figure 3A)**. EC_{50} values were left shifted by almost one log-unit (**Figure 3B**). In side-by-side experiments, RAMP3, used as a negative control, had no impact on the α-MSH-promoted response. No response was observed after α-MSH challenge in the absence of SNAP-MC4R expression, showing that the response is indeed MC4R-dependent (**Supplementary Figure 5D**). The p63RhoGEF sensor is also unresponsive in cells not overexpressing $G\alpha_q$, both in the presence or absence of MC4R, showing that the observed increase in BRET is solely dependent of $G\alpha_q$ and no other G protein (**Supplementary Figure 5C**).

Second, we measured second messenger production downstream of $G\alpha_q$ activation. Using IP-One HTRF assay, which monitors inositol monophosphate (IP1) accumulation, a metabolite of inositol-1,4,5-trisphosphate (IP3), this latter being produced following phospholipase C (PLC) stimulation downstream of $G\alpha_q$ activation. We found that MRAP2 co-expression with MC4R yields a leftward shift in the concentration-response curve of α-MSH (**Figure 3C**). This MRAP2-promoted increase in Gq activation is also supported by NFAT-reporter assays, as a read-out of calcium production, which is typically associated with PLC activation downstream of Gq activation (**Supplementary Figure 2**). Overall, co-expression of MRAP2 in a 1+1 (**Supplementary Figure 3**) or 1+4 amount with respect to the receptor, yields a threefold decrease in EC_{50} of IP1 production (**Figure 3D**). The observation that, in contrast to the p63RhoGEF BRET assay, no increase in the maximal response was observed most likely reflects a saturation of the IP1 response that is an amplified signal.

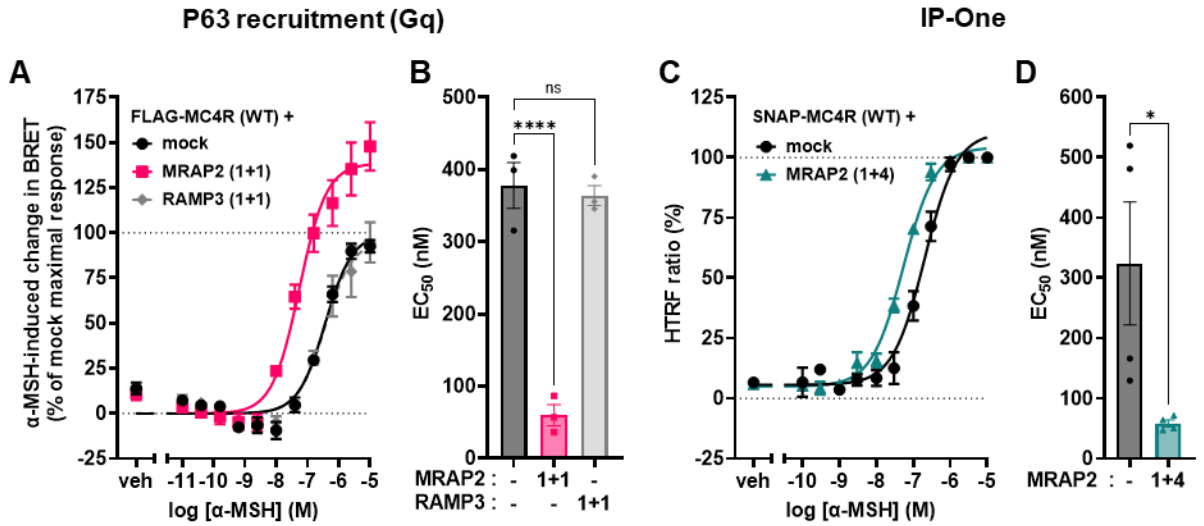

Figure 3: MRAP2 enhances Gq activation. (A) Mean concentration-response curves of the Gq-family selective effector p63RhoGEF-RlucII recruitment to the plasma membrane localization sensor rGFP-CAAX upon MC4R stimulation with α-MSH for 45 minutes, with overexpression of Gq in the presence or absence of MRAP2 or RAMP3 in transiently transfected HEK293-SL cells. MRAP2 or RAMP3 plasmid DNA is co-transfected with the same amount (1:1) with respect to MC4R DNA. **(B)** EC_{50} from the p63RhoGEF recruitment BRET experiments for Gq. Points represent average EC_{50} across the three independent experiments, and mean and SEM are indicated. Statistical analysis was performed using ordinary one-way ANOVA with Dunnett's multiple comparisons post-hoc test (**** = $p < 0.0001$). **(C)** Average concentration-response curves of IP-One assay upon MC4R stimulation using α-MSH, with and without MRAP2 1+4 DNA ratio with respect to MC4R, in transiently transfected HEK293T cells. Data are expressed as mean ± standard error of the mean (SEM) of four independent experiments. **(D)** EC_{50} values across all the replicates of the IP-One concentration-response curves for the two conditions. Points represent average EC_{50} across the four independent experiments, and mean and SEM are indicated. Statistical significance was calculated using an unpaired t-test (* = $p < 0.05$).

MRAP2 modulates MC4R constitutive and ligand-dependent internalization

It is becoming clear that changes in timing and location of GPCR signaling can alter cell response and physiology(Grundmann and Kostenis 2017). The observation that MRAP2 has a role in modulating the downstream signaling of MC4R suggests that one potential mechanism for MRAP2 to achieve this modulation might be to influence trafficking of MC4R. This question motivated us to investigate the role of MRAP2 expression in the localization and trafficking of MC4R.

First, we conducted a direct inspection of receptor localization by means of confocal microscopy. Labeling was achieved by a membrane impermeable dye (SNAP Surface Alexa Fluor 647) that irreversibly binds to SNAP-MC4R receptors on the plasma membrane. We then performed a pulse chase experiment that allowed us to monitor any labeled SNAP-MC4R that internalized during a 30-minute incubation period. Next, we compared the cellular distribution of the transfected SNAP-MC4R in HEK293 cells, in the presence or absence of MRAP2 co-expression (1+4). **Figure 4A** displays representative confocal micrographs: when SNAP-MC4R is expressed alone, considerable intracellular fluorescence is evident, due to receptor constitutive internalization during the incubation with the SNAP-tag dye. Notably, the intracellular signal largely disappears when co-expressed with MRAP2. In this case the expression pattern mimics the one observed upon preincubation for 30 minutes with 100 nM AgRP, an inverse agonist that should block constitutive internalization(Ollmann, Wilson et al. 1997). The use of AgRP in addition to MRAP2 co-expression did not significantly alter this pattern. Thus, it appears that MRAP2 effectively reduces constitutive MC4R internalization.

We then investigated MC4R internalization upon agonist stimulation. In HEK293T cells co-expressing SNAP-MC4R and the endosomal marker Cerulean-Rab5 (**Figure 4B, top**), we counted the number of endosomes within the cell before stimulation and 10 minutes after the addition of the agonist NDP-α-MSH at saturating concentrations (1µM). In both scenarios, MRAP2 expression decreases significantly the number of endosomes observed per cell (**Figure 4B, bottom**), as quantified in **Figure 4D.** Upon co-expression of MRAP2, there was no effect of NDP-α-MSH on the number of MC4R-positive endosomes per cells, suggesting an effective impairment of receptor internalization by MRAP2. This is paralleled by a reduction in the rate of receptor removal from the membrane upon agonist stimulation, illustrated in **Figure 4C.** Additional examples are shown in **Supplementary Figure 6.**

These results were complemented by an internalization readout, exploiting ebBRET between MC4R-RlucII and an acceptor rGFP fused to the FYVE zinc-finger domain of endofin, which acts as an early endosome targeting sequence (**Figure 4E**)(Namkung, Le Gouill et al. 2016). This approach, in which the addition of the RlucII in C-terminal of the MC4R does not perturb its function (**Supplementary Figure 1C**) allowed us to conduct a concentration response readout of MC4R internalization, comparing the effect of co-transfecting increasing amounts of MRAP2. Upon MRAP2 overexpression, either at a 1+1 or 1+4 ratio, there is a clear decrease in the BRET signal within the endosomes **(Figure 4E and 4F)**, again suggesting an impaired ligand-dependent internalization of MC4R in the presence of MRAP2. This is in stark contrast with measurements conducted using RAMP3 as a negative control, where this unrelated accessory protein has no effect on the internalization of MC4R.

Interestingly, when monitoring trafficking and cellular localization of MC4R in N7 murine embryonic hypothalamic cell line by confocal microscopy, these effects appeared to be amplified. N7 cells labeled with membrane impermeable SNAP-Surface® Alexa Fluor® 647 and expressing SNAP-MC4R, together with a cytosolic reporter displayed negligible plasma-membrane localization of the receptor (**Supplementary Figure 7A**). On the other hand, those cells expressed very well on the membrane the SNAP-β1-adrenoreceptor (SNAP-β1AR), another GPCR, used here as a positive control (**Supplementary Figure 7B)**.

When MC4R was co-transfected together with MRAP2 (1+1), it displayed a clear membrane localization, suggesting an even more prominent role of MRAP2 in regulating the trafficking of the receptor in this cell line in comparison to HEK293T cells consistent with its role in inhibiting constitutive endocytosis (**Supplementary Figure 7C)**.

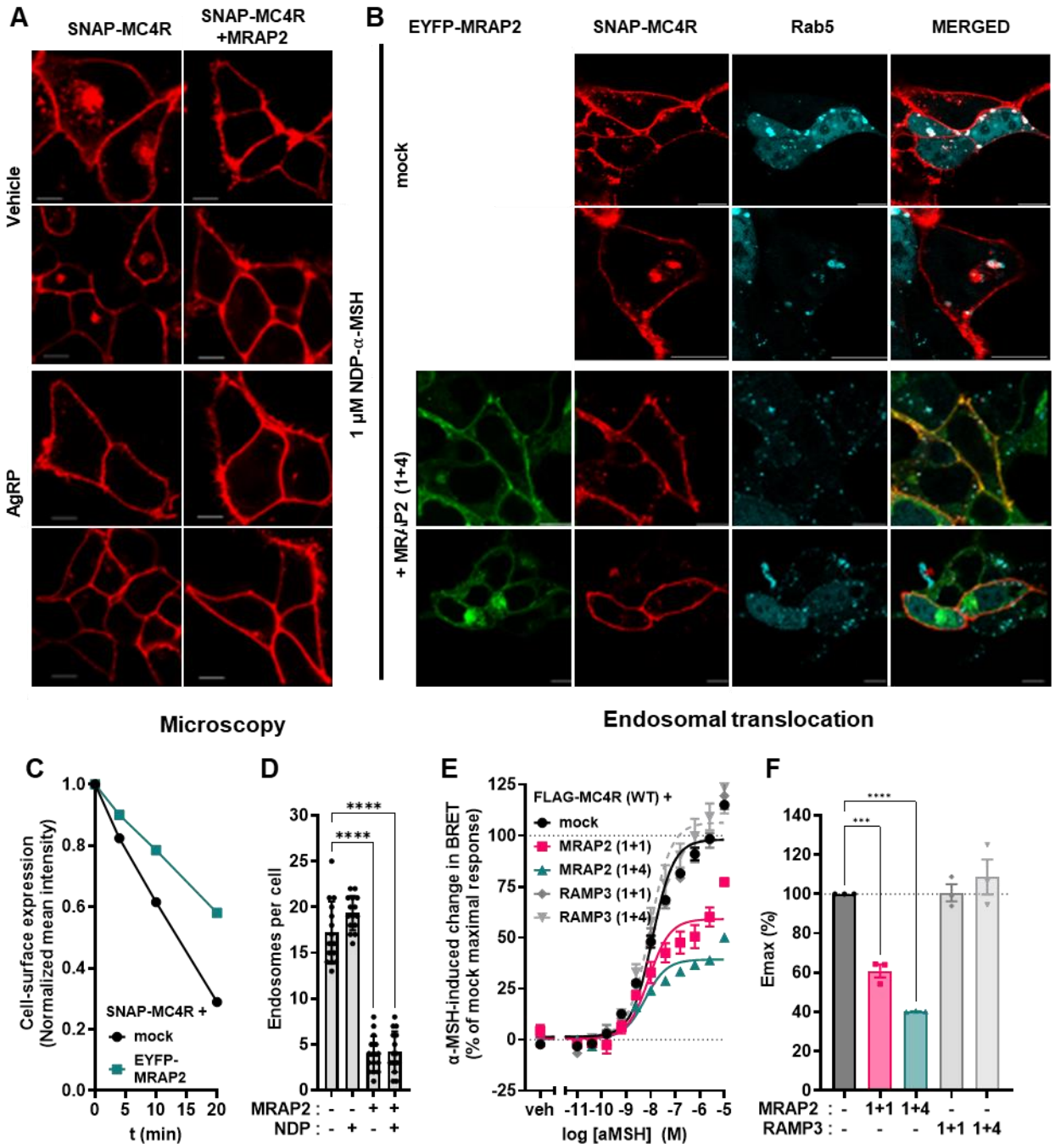

Figure 4: MRAP2 decreases constitutive and ligand-dependent endocytosis of MC4R. (A) Representative confocal micrographs of the localization and trafficking of SNAP-tagged MC4R in basal conditions or after the addition of 100 nM of the inverse agonist AgRP for 30 minutes in HEK293T cells in absence of presence of co-expression of MRAP2 (1+4). More than 3 independent experiments have been done. **(B)** Internalization of SNAP-tagged MC4R after 30 minutes incubation using NDP-α-MSH (1 µM), co-expressed with the endosomal marker Cerulean-Rab5, with or without co-expression of eYFP-MRAP2 (3 transfections, 14 cells). **(C)** Time evolution of SNAP-MC4R intensity at the plasma membrane of cells expressing SNAP-MC4R alone or in co-expression with eYFP-MRAP2 (1+4) upon stimulation with NDP-α-MSH (1 µM). Mean values ± 95% CI of at least three independent experiments are indicated. **(D)** Quantification of the number of endosomes per cell detected using Cerulean-Rab5 staining with and without co-expression of MRAP2 (1+4) together with MC4R, both in basal and agonist stimulated conditions).

Points represent technical replicates across the three independent experiments, and mean and SD are indicated. One-way ANOVA has been performed (**** = $p < 0.0001$. **(E)** Mean concentration-response curves of the translocation of MC4R-RlucII to the early endosome localization sensor rGFP-FYVE upon stimulation with α-MSH for 1 hour, in the presence or absence of MRAP2 or RAMP3 in transiently transfected HEK293-SL cells. MRAP2 or RAMP3 plasmid DNA is co-transfected with the same amount (1+1) or fourfold the amount (1+4) of the MC4R-RlucII plasmid DNA. Normalized data are expressed as mean ± SEM of three independent experiments. **(F)** E_{max} values from the translocation to early endosome BRET experiments. Points represent average E_{max} across the three independent experiments, and mean and SEM are indicated. Statistical analysis was performed using ordinary one-way ANOVA with Dunnett's multiple comparisons post-hoc test (*** = $p < 0.001$, **** = $p < 0.0001$).

Overexpression of MRAP2 decreases β-arrestin2 recruitment to the receptor

These results point to both enhanced Gs- and Gq/11-dependent downstream signaling, but, at the same time, a reduced trafficking and internalization rate. The latter led us to investigate if β-arrestin2 recruitment to the receptor, a canonical step following receptor activation that allows for clathrin-mediated endocytic internalization of the receptor for recycling and/or degradation, was affected by co-expression of MRAP2. We employed a luminescence-based protein complementation assay (NanoBiT), whereby luminescence from a complemented luciferase protein is observed upon close proximity of two proteins. In this case, the MC4R is fused with LgBiT at its C-terminus, whereas the β-arrestin2 is fused at its N-terminal with the SmBit(Janetzko, Kise et al. 2022).We observed that overexpression of MRAP2 at 1+1 ratio already leads to a significant decrease in β-arrestin2 recruitment directly to the receptor (**Figure 5A**). This reduction of β-arrestin2 recruitment in the basal state parallels the data of reduced constitutive internalization observed in our confocal microscopy quantification (**Figure 4A**). Furthermore, α-MSH stimulation results in reduced β-arrestin2 recruitment in the presence of MRAP2 (**Figure 5B**), mirroring the reduction of agonist-dependent MC4R internalization observed in the presence of MRAP2 (**Figure 4B**). These results are again recapitulated in an ebBRET assay conducted using a C-terminally labeled β-arrestin2-RlucII and the membrane targeted rGFP-CAAX (**Figure 5C**)(Namkung, Le Gouill et al. 2016). Here, for an equivalent amount of MRAP2 and MC4R transfected (1+1) and a fourfold excess of MRAP2 (1+4), we observed a substantial drop in E_{max} up to almost 40% whereas no change was observed upon co-expression of the negative control RAMP3. No change in BRET was detected in absence of SNAP-MC4R overexpression, showing the recruitment at the plasma membrane driven by MC4R (**Supplementary Figure 5B**).

These data suggest that the molecular mechanism of the interaction between MRAP2 and MC4R favors Gs- and Gq/11-coupling, while interfering with internalization, as well as β-arrestin2 coupling.

Despite the possible link between the increase in G protein signaling and the decrease β-arrestin2 recruitment and receptor endocytosis, we shall point out that the MRAP2-mediated increase in G protein signaling cannot be solely due to the β-arrestin-promoted endocytosis since a similar MRAP2-promoted leftward shift in Gs activation was observed in β-arrestin1 and β-arrestin2 double knock-out cells (**Supplementary Figure 8).**

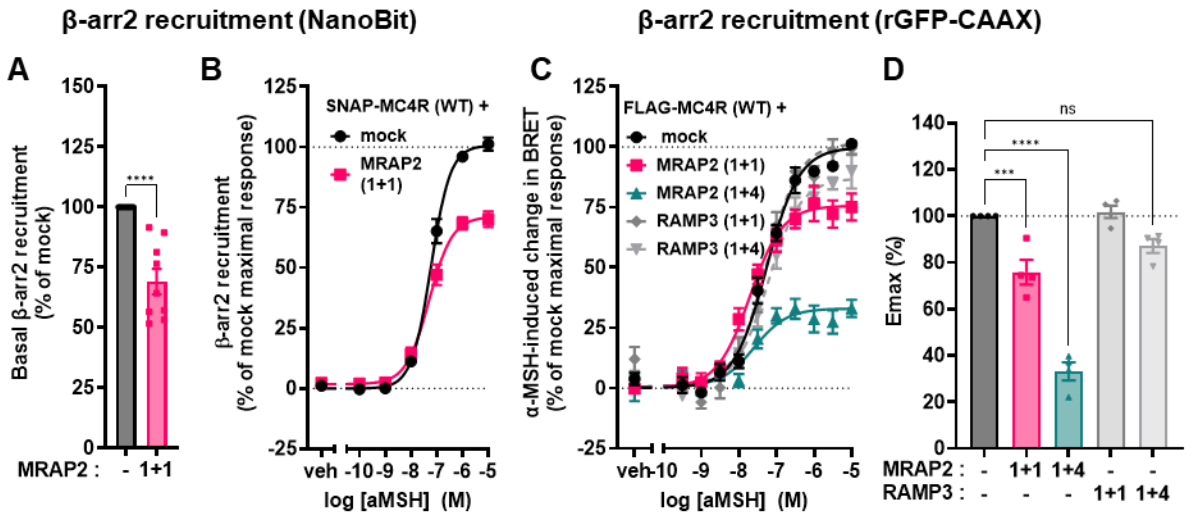

Figure 5: β-arrestin2 recruitment to MC4R in the presence or absence of MRAP2. (A) Bioluminescence-complementation based readout of SmBiT-β-arrestin2 recruitment to MC4R-LgBiT under basal conditions, with and without co-expression of MRAP2 (1+1). Data are expressed as percentage of the basal β-arrestin recruitment to the MC4R-WT in absence of MRAP2 (mock). Points represent average values across the nine independent experiments, and mean and SEM are indicated. Statistical analysis was performed with unpaired t-test (**** = $p < 0.0001$). **(B)** Average concentration-response curve of SmBiT-β-arrestin2 recruitment to MC4R-LgBiT upon α-MSH stimulation with and without co-expression of MRAP2 (1+1). Data represent mean ± SEM from three independent experiments with four replicates each. EC_{50} values and normalized maximal recruitment derived from curve fitting were 100% and 60 nM ± 8 nM for control condition and 67% and 50 nM ± 8 nM with overexpression of MRAP2 (1+1). **(C)** Mean concentration-response curves of β-arrestin2-RlucII recruitment to the plasma membrane localization sensor rGFP-CAAX upon MC4R stimulation with α-MSH for 2 minutes, in the presence or absence of MRAP2 or RAMP3 in transiently transfected HEK293-SL cells. MRAP2 or RAMP3 plasmid DNA is co-transfected with the same amount (1+1) or fourfold the amount (1+4) of the SNAP-MC4R plasmid DNA (140 ng), with total amount of DNA being constant. EC_{50} values were 58 ± 10 nM, 21 ± 4 nM and 32 ± 8 nM, respectively in the presence or absence of 1+1 or 1+4 MRAP2, and were not significantly different. Normalized data are expressed as mean ± SEM of four independent experiments. **(D)** E_{max} values from the β-arrestin2 recruitment BRET experiments. Points represent average E_{max} across the four independent experiments, and mean and SEM are indicated. Statistical analysis was performed using ordinary one-way ANOVA with Dunnett's multiple comparisons post-hoc test (*** = $p < 0.001$; **** = $p < 0.0001$).

MRAP2 expression alters the MC4R oligomeric equilibrium towards a monomeric state

Receptor oligomerization has long been a mechanism invoked to explain the modulation of GPCR downstream signaling, although less commonly this has been shown to influence the ligand-dependent response or to be in turn influenced by ligands(Isbilir, Moller et al. 2020) (Ferre 2015, Paradis, Feng et al. 2022). Based on BRET-based studies, we have previously suggested that the MC4R has a homodimeric arrangement(Reininghaus, Paisdzior et al. 2022), which can impact downstream signaling of the receptor, in particular coupling to Gs and Gq.

Thus, we tested the hypothesis that co-expression of MRAP2 can modulate the oligomeric state of MC4R. For this purpose, we performed a single-cell assay based on molecular brightness, similar to that used for other GPCRs(Isbilir, Serfling et al. 2021). We first conducted confocal microscopy of the basolateral membrane of cells expressing different receptor N-terminally tagged with SNAP-tag (**Figure 6A**) The brightness mean of the SNAP-β1AR was identified as a monomeric reference (**Supplementary Figure 9**), based on previous observation using this experimental method(Isbilir, Serfling et al. 2021). The fingerprint of the SNAP-MC4R, yielding a brighness approximately 1.7 times larger than a monomer, indicates a coexistence of higher order oligomeric species, averaging on an approximately dimeric condition (**Figure 6B**). However, co-expression of MRAP2 (1+4) leads to a change in the MC4R oligomeric fingerprint, and shifts the equilibrium towards a more monomeric population. Furthermore**,** MRAP2 appears to increase the average number of heterologously expressed MC4Rs (**Supplementary Figure 10**), in line with the observations reported in **Figure 4**.

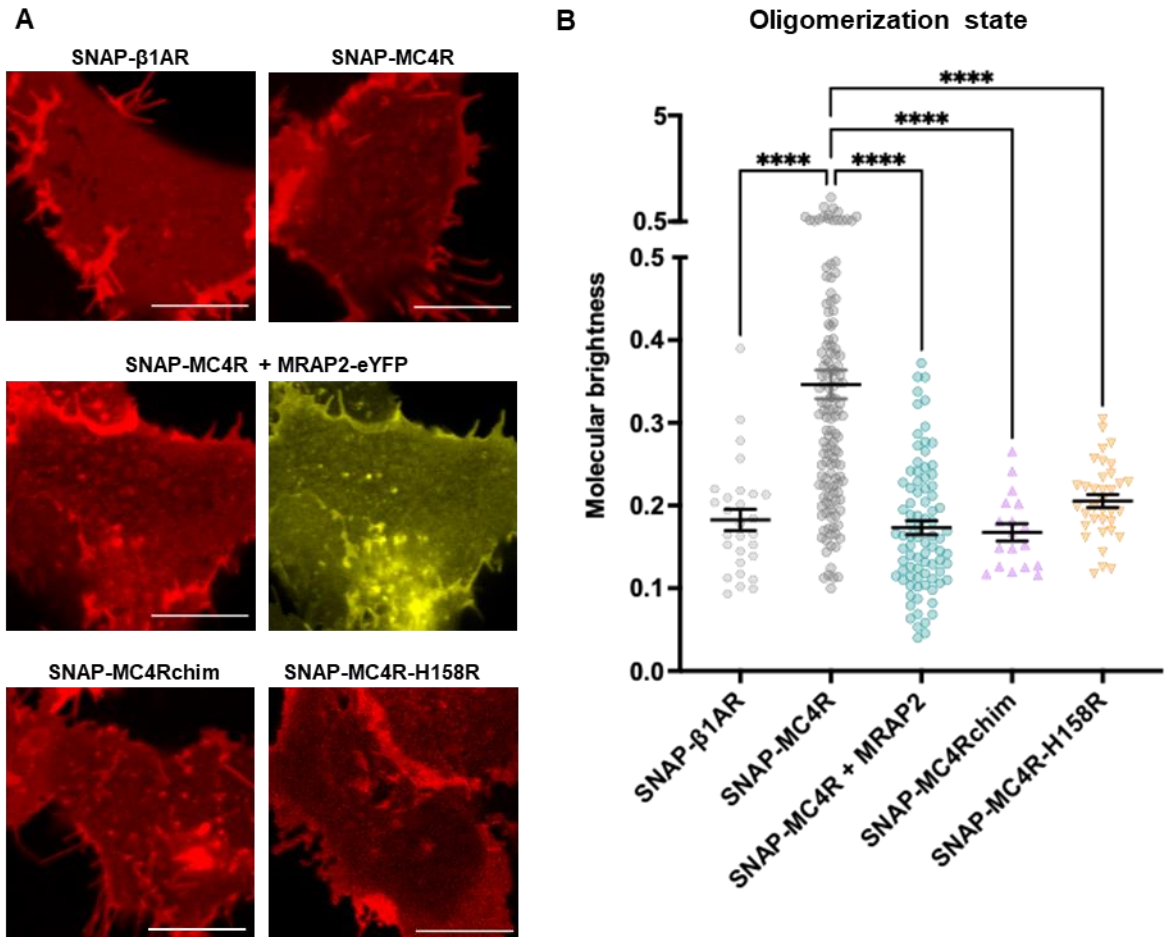

Figure 6: Oligomeric state of MC4R in the presence or absence of MRAP2. (A) Representative confocal micrographs of the basolateral membrane of HEK293 cells expressing SNAP-tagged GPCRs, all labeled using Alexa 647. From the top left the SNAP-β1AR (4 transfections, 28 cells), SNAP-MC4R (6 transfections, 135 cells), SNAP-MC4R in combination with eYFP-labeled MRAP2 (as a reference), SNAP-MC4R in presence of untagged MRAP2 (4 transfections, 85 cells), SNAP-MC4Rchim (3 transfections, 18 cells) and finally the SNAP-MC4R-H158R (3 transfections, 35 cells). **(B)** Molecular brightness values obtained for each of the control groups listed in **A**. Each dot represents the mean value from multiple regions of interest (ROIs) within a single cell. Several ROIs per cell were imaged. One-way ANOVA has been performed with Dunnett's multiple comparisons post-hoc test (**** = $p < 0.0001$). Mean ± SEM are shown in black.

Signaling of homodimerization-impaired MC4R variants is still affected by MRAP2

Our data delineate a scenario in which the MC4R is predominantly expressed as a dimer that will disassemble into a monomer upon interaction with MRAP2. This is accompanied by an increase in Gs and Gq activation, an elevated downstream cAMP and IP3 production, a decrease in β-arrestin2-mediated recruitment, and a significant reduction in receptor internalization.

This raises the question as to whether MC4R monomerization influences the receptor towards G-protein coupling, including both Gs and Gq, as opposed to β-arrestin2, or rather if the observed changes in signaling arise from a direct modulation of MC4R protomers by MRAP.

We tested this hypothesis by exploiting two modified MC4R that were already described having impaired homodimerization. The first one is the H158R natural variant of MC4R and the second one is a chimera (chim) engineered by replacing the ICL2 of MC4R by the one of the cannabinoid 1 receptor (CB1R)(Reininghaus, Paisdzior et al. 2022). We confirmed that both SNAP-tagged constructs were properly targeted to the plasma membrane using a membrane-impermeable SNAP dye (**Figure 6A**). Their monomeric nature was also confirmed by molecular brightness assay, although the SNAP-MC4R-H158R displayed a less marked monomeric fingerprint compared to SNAP-MC4Rchim (**Figure 6B**). We then tested the function of the MC4R-H158R mutant and the chimera using the Epac-S^{H187} FRET biosensor. The SNAP-MC4R-H158R displayed comparable E_{max} and EC_{50} to the SNAP-MC4R-WT in response to α-MSH (**Figure 7A**), as well as a similar behavior as the SNAP-MC4R-WT in response to co-expression of MRAP2 (1+1), namely a left-shift of the EC_{50} (**Figure 7B**). The response of SNAP-MC4Rchim could not be assessed as the maximal response reached the forskolin control and therefore we could not exclude that the assay was saturated. We could however observe a substantial increase in constitutive activity for the chimera (**Figure 7C**).

We conducted parallel experiments using the ebBRET-based miniGs recruitment assay, after verifying that the N-terminal FLAG-tag did not perturb MC4R function (**Supplementary Figure 1C**). Consistent with the FRET data, both the FLAG-MC4R-H158R (**Figure 7E**) and FLAG-MC4Rchim (**Figure 7F**) displayed comparable activation to the FLAG-MC4R-WT (**Figure 7D**) in response to MRAP2 co-expression (both 1+1 and 1+4), namely a shift to the left in EC_{50} and a reduction in E_{max} (**Supplementary Figure 8**). Altogether, these results seem to indicate that the observed effects of MRAP2 on MC4R signaling, namely increased Gs and Gq signaling (**Figure 1** and **Figure 3**), occur primarily due to an interaction between MRAP2 and the MC4R protomer.

Finally, we tested the ability of the MC4R-H158R and the chimera in the presence of the absence of MRAP2 to recruit β-arrestin2 by BRET assays. Interestingly, both the FLAG-MC4R-H158R (**Figure 7H)** and the FLAG-MC4Rchim (**Figure 7I**) displayed a sizable reduction of β-arrestin2 recruitment (E_{max}) to the plasma membrane marker rGFP-CAAX in response to α-MSH. The hampered β-arrestin2 recruitment was even more pronounced for the MC4Rchim (**Figure 7I**). For both the mutant and the chimera, co-expression of MRAP2 (1+1) led to virtually no change in recruitment, whereas co-expression of MRAP2 in a (1+4) ratio led to a reduction in E_{max}, akin to the behavior observed for miniGs recruitment.

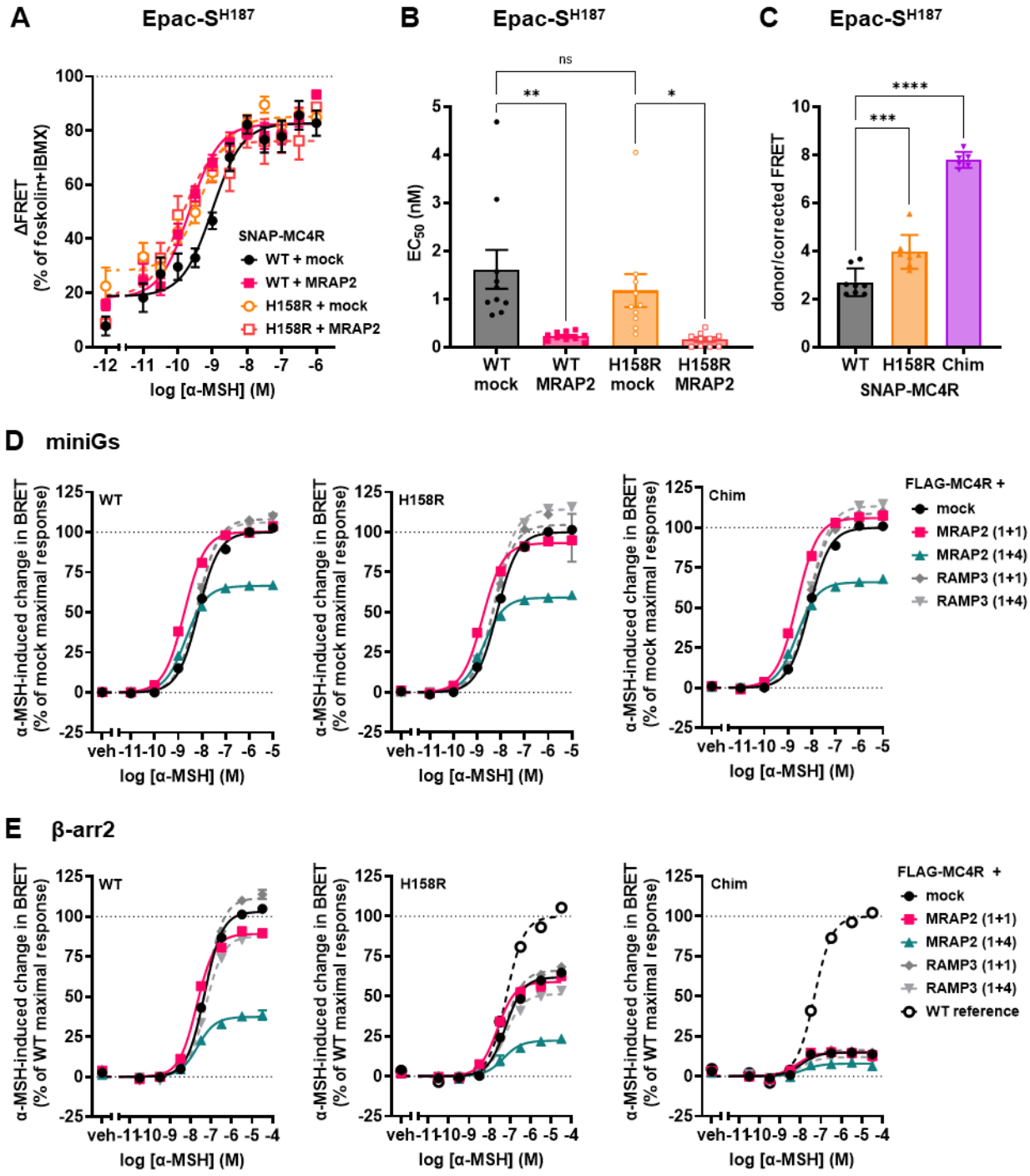

Figure 7: Signaling profile of monomeric MC4R mutant and MC4R chimera are altered by co-expression of MRAP2 . (A) Average concentration-response curve of cAMP response using α-MSH in transiently transfected HEK293 cells expressing SNAP-MC4R and MC4R-H158R, in the presence or absence of co-transfection with MRAP2 in a 1+1 ratio. ΔFRET values are normalized to forskolin response in the presence of phosphodiesterase inhibitor IBMX. Mean ± SEM for at least three independent expriments (containing each three technical replicates) are shown. **(B)** EC_{50} values obtained using the Epac-S^{H187} FRET biosensor. Points represent average EC_{50} across at least three independent experiments, and mean and SEM are indicated.

One-way ANOVA has been performed with Dunnett's multiple comparisons as post-hoc test (* = $p< 0.05$, ** = $p< 0.01$). **(C)** Constitutive activity of the MC4R-H158R and the MC4Rchim. Points represent technical replicates expressed in donor/corrected FRET ratio across at least three independent experiments, and mean and SD are indicated. **(D)** Average concentration-response curves of Rluc8-miniGs recruitment to the plasma membrane localization sensor rGFP-CAAX upon stimulation of FLAG-hMC4R-WT, FLAG-hMC4R-H158R or FLAG-MC4Rchim with α-MSH for 45 minutes, in absence or presence of MRAP2 or RAMP3 in transiently transfected HEK293-SL cells. BRET values are normalized to maximal response obtained with mock condition. Data are expressed as mean ± SEM of four independent experiments. **(E)** Average concentration-response curves of β-arrestin2 recruitment to the plasma membrane localization sensor rGFP-CAAX upon stimulation of FLAG-hMC4R(WT), FLAG-hMC4R-H158R or FLAG-MC4Rchim with α-MSH for 2 minutes, in absence or presence of MRAP2 or RAMP3 in transiently transfected HEK293-SL cells. BRET values are normalized to maximal response obtained with FLAG-hMC4R-WT. MRAP2 or RAMP3 plasmid DNA is co-transfected with the same amount (1+1) or fourfold the amount (1+4) of the FLAG-hMC4R plasmid DNA in their respective assay. Data are expressed as mean ± SEM of three independent experiments. Parameters graphs are displayed in **Supplementary Figure 9**.

Putative MC4R–MRAP2 interaction sites

In order to understand how a MC4R monomer/MRAP2 monomer complex might be constituted and influence receptor signaling, we generated a putative structural homology model of an active MC4R–MRAP2–Gs protein complex with an agonistic ligand. This is supported by the sequence homology between MRAP2 and MRAP1 (**Supplementary Figure 12** and between MC2R and MC4R **(Supplementary Figure 13**). In this homology model, the heterodimer interface is predicted to be between the transmembrane helices (TMH) 5 and 6 of MC4R and the membrane-spanning helix of MRAP2. Similarly to the MC2R-MRAP1 complex, additional interactions of the MRAP2 N-terminus with the extracellular loop 3 (ECL3), the TMH7 and the N-terminus of MC4R can be inferred (magenta arrows in **Figure 8**).

Of particular note, structural information on the MC2R–MRAP1 complex (PDB ID: 8gy7) does not contain the full-length MRAP1, as the complete intracellular C-terminal tail is missing. This, in turn, precludes any prediction of a potential impact on G protein coupling or homodimerization in the MC4R-MRAP2 homology model. In addition, presumed antiparallel MRAP homodimer formation is not included in the model as it was not observed in the MC2R-MRAP1 structural template.

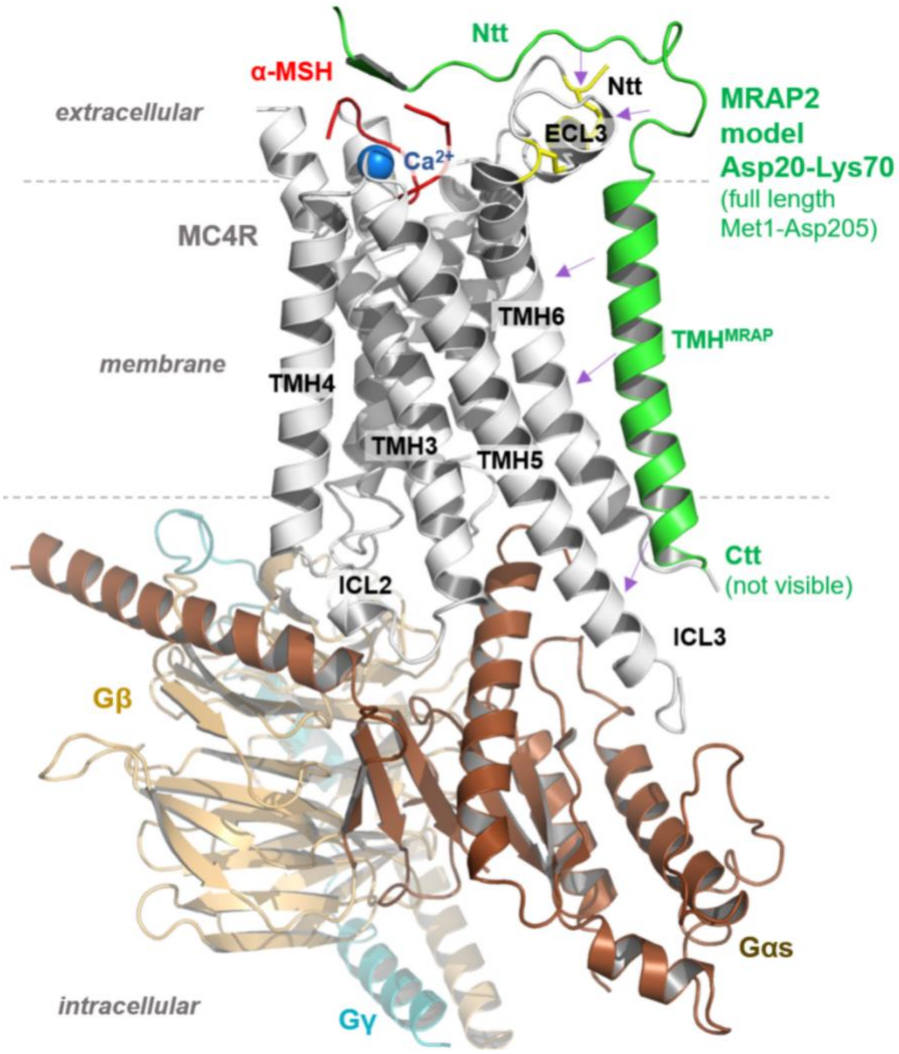

Figure 8: Structural model of an active state MC4R-MRAP2 complex. In this model α-MSH (red surface) interacts with the MC4R between the transmembrane helices (TMH) and interconnecting extracellular loops (ECL) as described recently(Heyder, Kleinau et al. 2021, Zhang, Chen et al. 2021), together with the essential co-binding factor calcium (blue sphere). The heterotrimeric Gs protein couples intracellularly at the agonist bound MC4R conformation. MRAP2 (green) contacts to MC4R are supposed at TMH5, TMH6, ECL3 and the N-terminus (Ntt) (arrows).

DISCUSSION

In this study, we have provided novel insight into the molecular mechanisms that underlie the action of MRAP2 on MC4R cellular function. Using real-time signaling assays, single molecule microscopy approaches, and molecular modeling we demonstrate that MRAP2: (*i)* enhances MC4R signaling for at least two different G protein-driven signaling pathways; *(ii)* decrease the recruitment of β-arrestin; *(iii)* modulates MC4R cellular trafficking, *(iv)* modulates the oligomeric state of MC4R; and (*v*) enhances Gs-mediated signaling for at least two monomeric forms of MC4R. These findings shed light on how MRAP2 has a direct and modulatory influence on the MC4R, and thus represents a potential important regulator of MC4R-associated functions such as energy consumption and appetite regulation.

The identification of the first human *MRAP2* mutations found in obese patients highlighted the role of MRAP2 in modulating MC4R signaling (Asai, Ramachandrappa et al. 2013, Schonnop, Kleinau et al. 2016, Baron, Maillet et al. 2019). It was presumed that MRAP2 would function analogously to RAMPs, that can modulate GPCRs by influencing their trafficking to the cell surface, expression, ligand binding, signaling and internalization. Towards this end, an intense effort has been undertaken to understand the role of MRAP2 on these aspects of MC4R physiology and function. In particular, a role of MRAP2 in reducing the capacity of MC4R to form dimers/oligomers was speculated, but until now not experimentally validated(Reininghaus, Paisdzior et al. 2022).

Our findings that MRAP2 increases the capacity of MC4R to activate different G protein subtypes begs the questions (*a*) is this a true reflection of physiology and (*b*) how this might be achieved. In support of the former, there is a precedent for these findings in previous studies that demonstrated a reduction of MC4R signaling in the presence of loss-of-function MRAP2 mutations(Asai, Ramachandrappa et al. 2013, Schonnop, Kleinau et al. 2016, Baron, Maillet et al. 2019). In addition, a more specific increase in Gs and Gq activation by MC4R was observed in HEK293 cells that stably express MRAP2(Metzger, Zhang et al. 2024). Interestingly, we could also detect a major increase in signaling with $G\alpha_{15}$, another G protein from the Gq/11 family (**Supplementary Figure 5D**). PTX-sensitive activation of endogenous MC4R in GT1-7 murine hypothalamic cell-line was previously described, suggesting that Gi activation can be detected in some systems(Buch, Heling et al. 2009). It would be interesting to see the impact of MRAP2 on Gi pathways.

The potential mechanisms behind the increase in G protein signaling are still opaque, but can be inferred by some of our additional findings in this study.

One possibility is that the increase in the potency to activate G protein would be due to the breakage of the MC4R homo-oligomers, as many dimerization-impaired mutants and engineered chimera were already described to have enhanced G protein signaling. We indeed showed that MRAP2 was able to impact the MC4R monomer-dimer equilibrium, pushing the equilibrium toward a monomeric state (**Figure 6B**). However, we also discovered that homo-dimerization-deficient MC4R-H158R and MC4Rchim display normal Gs signaling in absence of MRAP2 and enhanced Gs signaling in the presence of MRAP2, mimicking the WT receptor behavior (**Figure 7)**. Those data suggest that the effects of MRAP2 on the G protein potency would arise from its specific interaction with the protomer rather than on the breakage of the MC4R homo-oligomers. This is also in line with the observation that at a higher ratio, MRAP2 decreases the E_{max} of miniGs recruitment towards the WT (**Figure 2**), as well as towards both the MC4R-H158R and MC4Rchim (**Figure 7**). This is further supported by the observation that α-MSH binding is enhanced in MRAP2-positive cells, suggesting an increased affinity for the agonist (**Supplementary Figure 4**).

At the same time, the scenario appears to be more complex: MRAP2 decreases the recruitment of β-arrestin2 at the now monomeric MC4R-WT, and the decrease in β-arrestin recruitment at the MC4R-H158R and the MC4Rchim is aligned to the shift of the oligomeric equilibrium towards the monomeric state. In other words, MC4Rchim has a stronger monomeric fingerprint (**Figure 6**) and a worse β-arrestin recruitment (**Figure 7** and **Supplementary Figure 9)** than MC4R-H158R. These results are in line with recent data on the impact of the oligomerization or the oligomer-protomer conformation on β-arrestin engagement of the CXCR4(Paradis, Feng et al. 2022) and dopamine 2 receptor (D2R)(Sharrocks, Fanelli et al. 2024). These possibilities of the impact of the oligomerization state shed light on the intricate mechanisms underlying GPCR signaling regulation and warrant further investigation.

The reduction in β-arrestin recruitment could lead to reduced receptor desensitization, which would in turn favor G protein signaling. However, the presence of MRAP2 induced the same left-shift in the α-MSH-promoted miniGs recruitment in β-arrestin1 and β-arrestin2 double knock-out cells (**Supplementary Figure 8**). Those data suggest that β-arrestins play a negligeable role in the increase in G protein coupling potency.

As expected with reduced β-arrestin recruitment(Brouwers, de Oliveira et al. 2021), we also show that MRAP2 co-expression also impairs receptor endocytosis, which would typically result in a build-up of receptors at the cell surface, enhancing G protein signaling responsiveness. We indeed have observed an increase in MC4R cell-surface expression upon co-expression of MRAP2 in HEK293 (**Supplementary Figure 9**), which positively correlates with the amount of MRAP2 detected in the cells (**Supplementary Figure 4C**). This effect is even more striking in N7 cells, an embryonic mouse hypothalamic cell-line, in which MC4R is mostly observed intracellularly in absence of MRAP2 (**Supplementary Figure 7**). This could be either be attributed to a decrease in endocytosis or to an increased in cell-surface targeting of MC4R from the secretory pathway, akin to what observed for MRAPs and the MC2R (Webb and Clark 2010).

In order to understand at the molecular level how MRAP2 could achieve such an impact on MC4R, we developed a homology model between MRAP2 and MC4R. This model indicates potential interaction sites between MRAP2 and MC4R at TMH5, TMH6 and the TMH7-ECL3 transition (**Figure 8**). While so far it is unknown how MC4R homodimers are exactly constituted, TMH5 and TMH6 have been identified from various GPCR-GPCR dimer structures as potential interaction sites between the protomers(Navarro, Cordomi et al. 2016), as in the CXCR4 homodimer (PDB ID: 3ODU(Wu, Chien et al. 2010)), or the μOR homodimer (PDB ID: 4DKL(Manglik, Kruse et al. 2012)). In consequence, binding of MRAP2 at this region should compete with dimerization (or oligomerization) of MC4R.

Moreover, TMH5 and TMH6 of GPCRs are structural rearrangement hot-spots during receptor activation(Weis and Kobilka 2018), with the highest importance known for TMH6(Weis and Kobilka 2018). Our MC4R–MRAP2 model suggests an interaction of both TMH5 and THM6 of MC4R with the transmembrane helix of MRAP2.This interaction could further imply an increased retention of the active state, which might allow for better G-protein coupling observed in our experiment(Paradis, Feng et al. 2022).On the other hand, the TMH5-ICL3-THM6 axis is presumably also important for the spatial adjustment of the arrestin at the receptor. Considering that MRAP2 impairs β-arrestin2 recruitment in our assays, MRAP2 could thus influence the binding of the arrestin as an interfering factor, an aspect that has already been suggested for PKR1(Lattanzi, Casella et al. 2024). However, as the intracellular loop 3 (ICL3) remains unresolved in our homology model based on the MC2R-MRAP1 structure, it is difficult to predict how this loop would interact with MRAP2.

The increase in potency in activating G proteins could therefore be explained by the increase in affinity for the ligand and/or active state retention by the MRAP2. On the other hand, the decrease in β-arrestin recruitment could be attributed to the breakage of the dimer or a steric hindrance from the MRAP2. However, this model does not recapitulate entirely all our observations, since the decrease in maximal miniGs recruitment caused by MRAP2 at a ratio of 1+4 remains unexplained, suggesting the need of further investigations to fully understand the broad and complex repertoire of MC4R regulation by MRAP2.

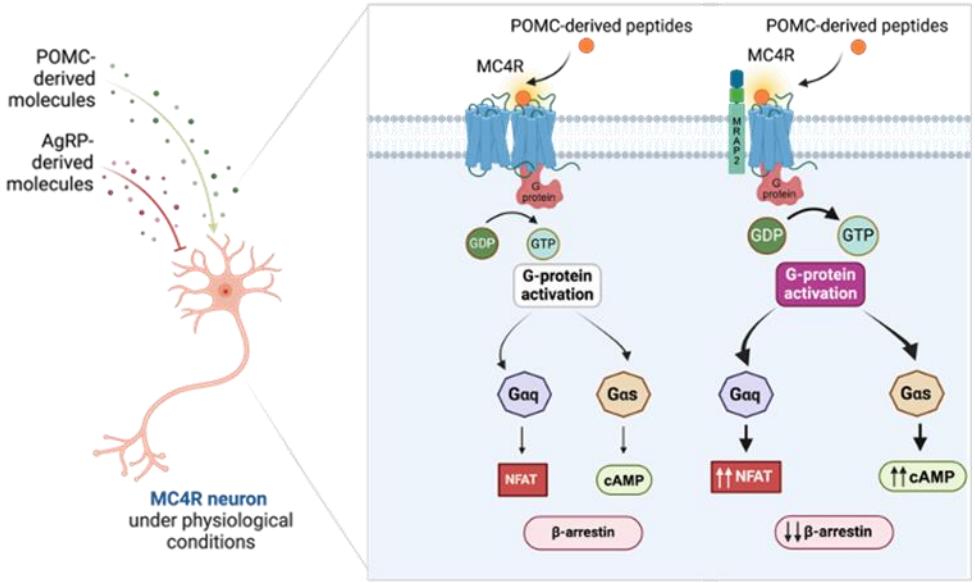

Figure 9: Effects of MRAP2 at the MC4R. The MC4R is activated by POMC-derived peptides from POMC-neurons the nucleus arcuatus, left side. In addition, AgRP/NPY neurons of the nucleus arcuatus produce AgRP which is in turn axonally transported to the PVN where the function of the MC4R is modulated by AgRP and POMC-derived peptides. Constitutively, the MC4R is in a higher oligomeric state at the plasma membrane of cells (square, left side). As such, it can interact with Gs and Gq as well as β-arrestin2, both constitutively as well as in response to POMC-derived molecules such as α-MSH and result in internalization. Upon co-expression of MRAP2 (square, right side), the equilibrium shifts in favor of monomers. Moreover, the interaction with MRAP2 favors Gs and Gq coupling, whereas ligand-dependent β-arrestin2-recruitment is impaired. These processes are further accompanied by a reduction in constitutive and ligand-dependent internalization.

Final remarks

In summary, our results demonstrate the important role of MRAP2 in modulating MC4R signaling cascades in response to stimulation by the endogenous agonist α-MSH, as well as its synthetic analog NDP-α-MSH, and alterations to the monomer-dimer equilibrium. Albeit monomerization of MC5R by interaction with MRAP1 has been previously shown(Sebag and Hinkle 2009), our observations at MC4R provide new findings directly showing an effect of MRAP2 in regulating an oligomeric GPCR state, which has not been shown experimentally before. While our results showing reduced β-arrestin2 engagement by monomeric mutant MC4R-H158R and MC4R-CB1R chimera are in line with recent publications on the role of oligomerization in this process, more investigation will be needed to make a causal link in the case of MC4R.

Considering these results at the physiological level, MRAP2 expression can play an important role in the modulation of cellular signaling. Here, the important question would be what modulates MRAP2 expression in those cell types or neurons that express MC4R over an individual's lifetime and if MRAP2 expression is modulated by food intake or lack thereof in times of famine of food surplus. Cell-type specific expression of MRAP2 emerges thus as an additional tool that organisms can use to modulate and bias GPCR signaling in a context-dependent fashion(Bernard, Ojeda Naharros et al. 2023). For example, it was already evidenced that co-expressed MRAP2 increases ACTH binding and signaling at MC4R, in contrast to α-MSH(Josep Agulleiro, Cortes et al. 2013, Soletto, Hernandez-Balfago et al. 2019). This may contribute to a higher spectrum of MC4R-related effects, dependent on the simultaneous expression of MRAPs.

Taken together, our results point to a more complex physiological system for the regulation of MC4R-mediated pathways controlling metabolism and satiety, which we expect to be reflected also at the neuronal level. Our data pave the way to test this concept for other GPCRs where signal modulation through interaction with either MRAP1 or MRAP2 has been observed(Wang, Wang et al. 2022).

Acknowledgments

We thank Sabine Jyrch for excellent technical assistance. We would like to thank Alexei Sirbu for his helpful support. This work was supported by the Deutsche Forschungsgemeinschaft (DFG) (German Research Foundation) through SFB1423, Project-ID 421152132, subprojects C03 (to P.A., M.J.L), B02 (to H.B.), A01/Z03 (to P.S.). P.A. would like to acknowledge generous funding from the Leverhulme Trust RL-2022-015. Funding was received through Germany's Excellence Strategy – EXC 2008 – 390540038 – UniSysCat (Research Unit E) (to G.K. and P.S.) and by the European Union's Horizon 2020 Research and Innovation Programme under the Marie Skłodowska-Curie grant agreement No 956314 [ALLODD] (to P.S.). UKRI funding to P. McC. CIHR funding (PJT-183758) to M.B. FRQS PhD scholarship to S-A.L. We thank Advanced light microscopy (ALM) facility at MDC, Buch.

Author Contributions

H.B., P.McC, M.B. and P.A. designed research

I.S., S-A.L, V.C., A.S., Z.C.U.K., P.S., G.K. performed research

A.M. and J.T. performed research

I.S., S-A.L, V.C., P.A., A.M., Z.C.U.K, H.B., M.B. data analysis

G.K. and P.S. performed, analyzed and visualized structure and sequence analysis

I.S., V.C., P.A., H.B., graphical analysis

I.S., H.B., P.McC., G.K., P.S., M.J.L, P.A., S-A.L M.B. wrote and revised the manuscript

H.B., P.McC., P.A., M.B. supervision of experiments

H.B., P.A., M.J.L., P.S., M.B funding acquisition

SUPPLEMENTARY MATERIALS

Supplementary Figures and Tables

Protein	nTMP	MC4R:MRAP2
MC4R	3.6	1:3
MRAP2	11.5	

Supplementary Table 1: The normalized gene expression values (nTMP) representing the RNA expression of the MC4R and MRAP2 in the paraventricular nucleus of the hypothalamus (The Human Protein Atlas, 2023). The values obtained give an expression ratio for MC4R to MRAP2.

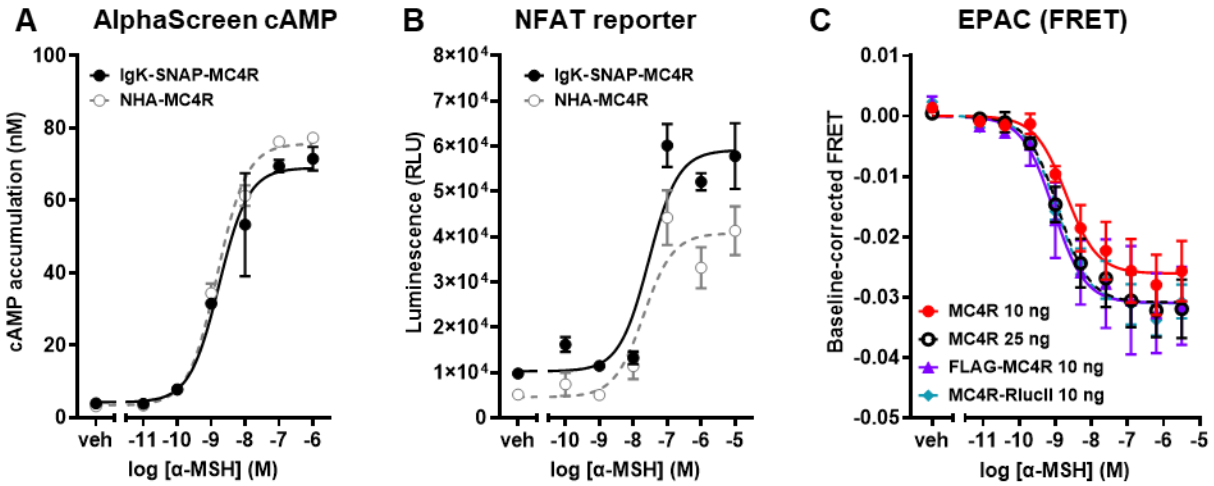

Supplementary Figure 1 : N-terminal and C-terminal tags used in this study do not impair MC4R downstream signaling. (A) N-terminal SNAP-tag doesn't impair cAMP accumulation, as assessed with AlphaScreen technology (ref), **(B)** nor does it impair PLC activation, as assessed with NFAT-induced luminescence, as compared to N-terminal HA-tag MC4R (see Materials and Methods). **(C)** N-terminal FLAG-tag or C-terminal RlucII- tag do not impair cAMP production elicited by stimulation by α-MSH for 25 minutes compared to untagged MC4R, as assessed with sCFP3A-EPAC-Venus cAMP FRET biosensor . Data are expressed as mean ± SEM of three independent experiments.

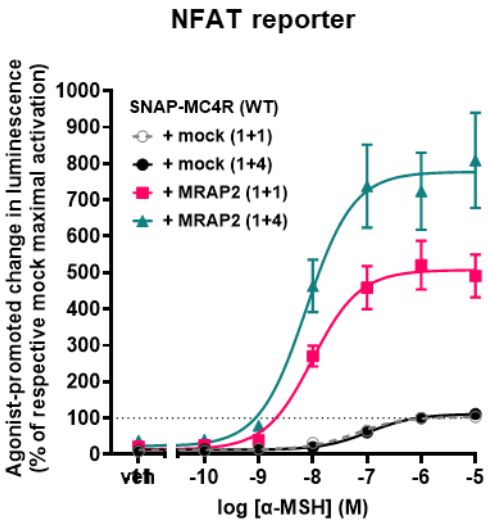

Supplementary Figure 2: Activation of phospholipase C activation via NFAT reporter gene assay. In order to determine the effect of MRAP2 on phospholipase C activation MC4R and indicated ratios of MRAP2 and NFAT reporter were co-transfected into HEK293 cells. 48 h after transfection cells were stimulated with increasing amounts of α-MSH for 6h and luciferase activity was determined. The result of 8 independent experiments performed in triplicates is shown (mean ± SEM).

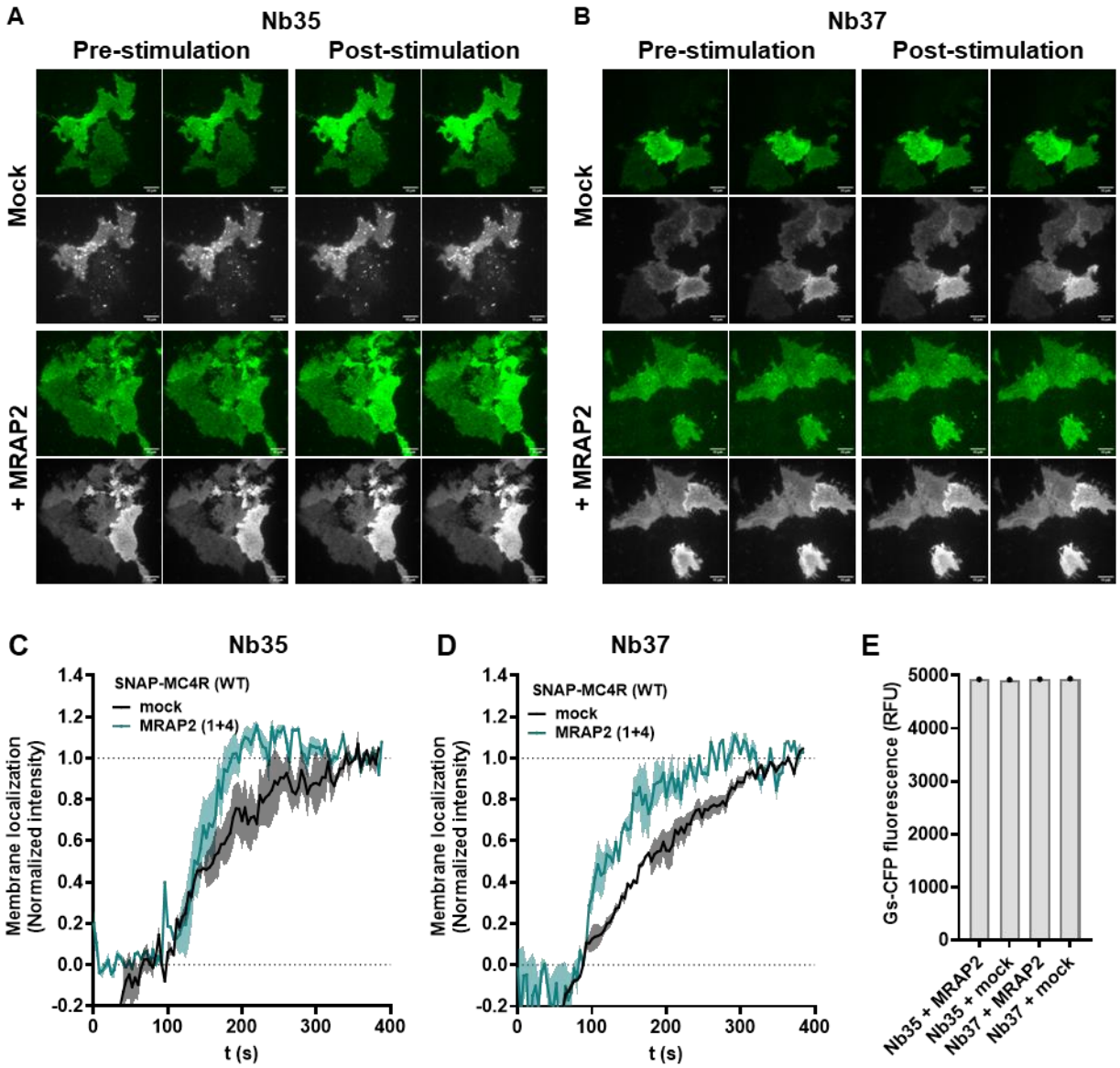

Supplementary Figure 3: Recruitment of Nb35 and Nb37 in HEK293 cells heterologously expressing SNAP-MC4R +/- MRAP2 and Gs. Recruitment of **(A)** Nb35-eYFP or **(B)** Nb37-eYFP to cerulean-Gs-positive cells with and without MRAP2 (1+4). SNAP-MC4R labeled with SNAP-Surface 647 (gray) and Nb35-eYFP (green). Kinetic of the intensity of **(C)** Nb35-eYFP or **(D)** Nb37-eYFP measured at the plasma membrane of HEK293AD cells using TIRF, with and without MRAP2. **(E)** Fluorescence intensity (arbitrary intensity units) in the cyan channel from populations of cells co-transfected with Gs-CFP plasmid and the constructs indicated. No fluctuation in the expression level of $G\alpha_s$ is observed (n=1).

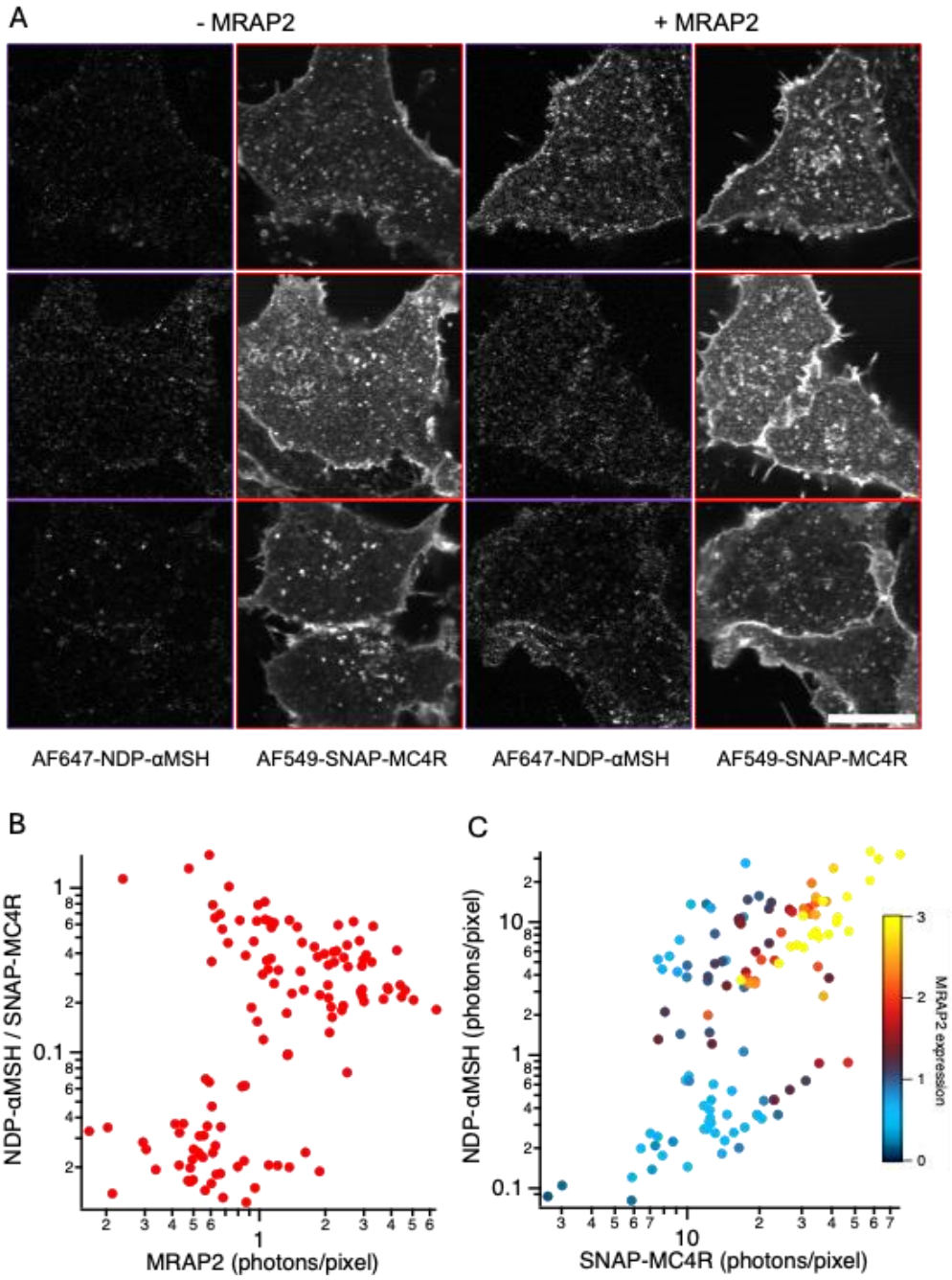

Supplementary Figure 4: Binding of NDP-α-MSH is increased HEK293 expressing MRAP2. (A) Confocal maximum intensity projections of representative HEK293 cells transfected with either SNAP-MC4R + mock or SNAP-MC4R + MRAP2 (1+4), seeded on the same coverslip and then labeled using SNAP-surface549. The cells were then incubated for 5 minutes with 0.5nM Alexa647-NDP-α-MSH and imaged. Contrast is set to the same values in each channel. Maximum intensity projections were constructed in FIJI before running Cellpose-based cell segmentation to extract individual cells intensity values. Scale bar is 10 µm. **(B)** Chart of the normalised NDP-αMSH ligand signal (to SNAP-MC4R receptor expression) per cell (n=1 independent transfection, 121 cells). **(C)** Chart of ligand signal as a function of receptor expression, color coded according to MRAP2 expression levels.

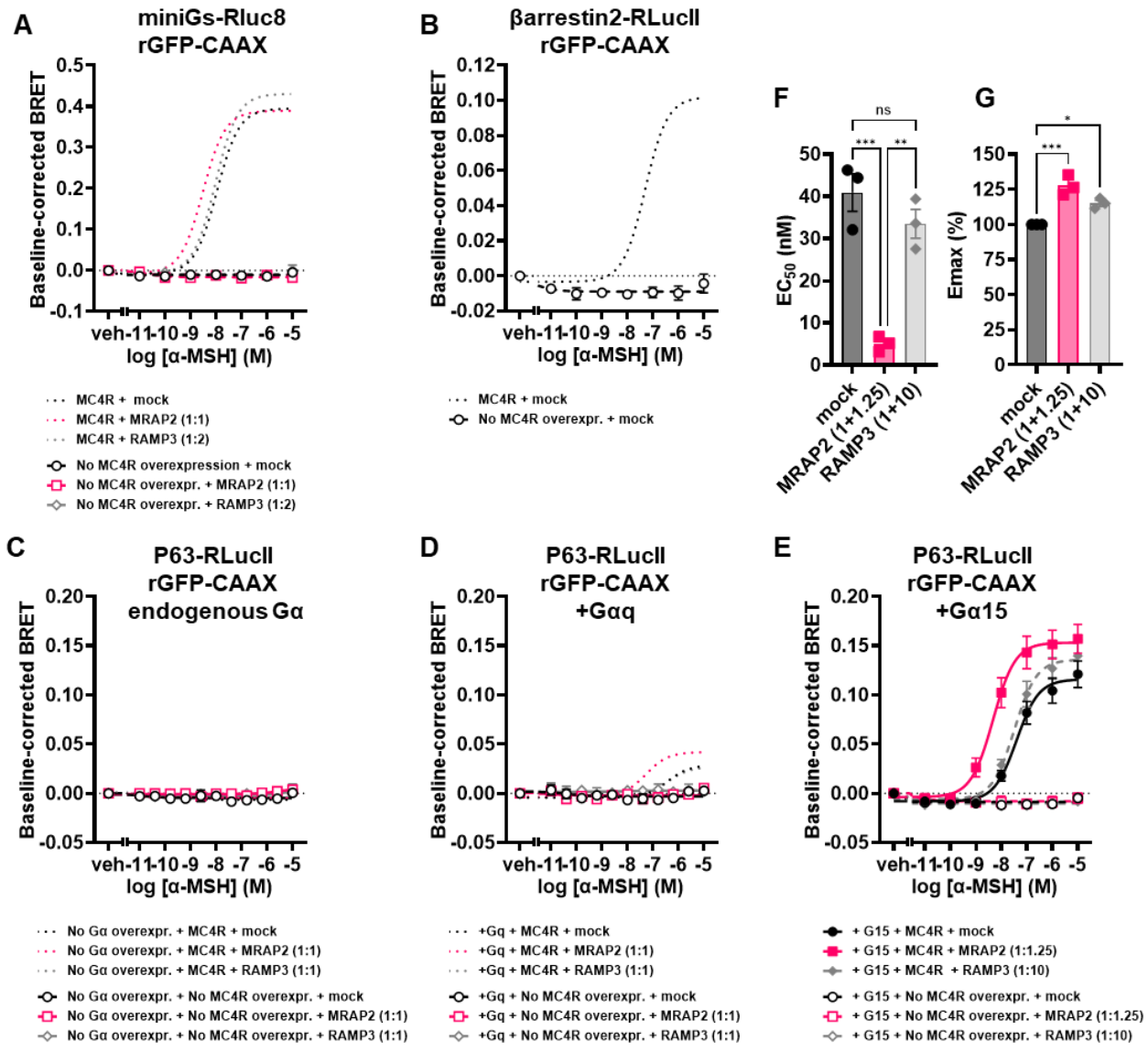

Supplementary Figure 5: Complementary BRET experiments. Mean concentration-response curves of BRET sensor stimulation with α-MSH, without or with overexpression of SNAP-MC4R in the same set of experiments unless stated otherwise, in the presence or absence of MRAP2 or RAMP3 at the indicated ratio with respect to MC4R, in transiently transfected HEK293-SL cells. Baseline-corrected (agonist-promoted change in BRET) responses are expressed as mean ± SEM of three independent experiments. **(A)** Rluc8-miniGs recruitment to the plasma membrane localization sensor rGFP-CAAX after 45 minutes of stimulation. Curves from Figure 2C are represented in dotted lines for scale reference. **(B)** β-arrestin2-RlucII recruitment to the plasma membrane localization sensor rGFP-CAAX after 3 minutes of stimulation. This experiment was carried independently of the one presented in the main text. **(C-E)** Gq-family selective effector p63RhoGEF-RlucII recruitment to the plasma membrane localization sensor rGFP-CAAX after 45 minutes of stimulation, **(C)** in the presence or absence of overexpression of **(D)** $G\alpha_q$ or **(E)** $G\alpha_{15}$. Curves from Figure 3A are represented dotted lines for scale reference in panel D. **(F)** EC_{50} and **(G)** E_{max} from the p63RhoGEF recruitment experiments for Gq. Points represent average EC_{50} and E_{max} values across the three independent experiments, and mean and SEM are indicated. Statistical analysis was performed using ordinary one-way ANOVA with Dunnett's multiple comparisons post-hoc test (* = $p < 0.05$, ** = $p < 0.01$, *** = $p < 0.001$, **** = $p < 0.0001$).

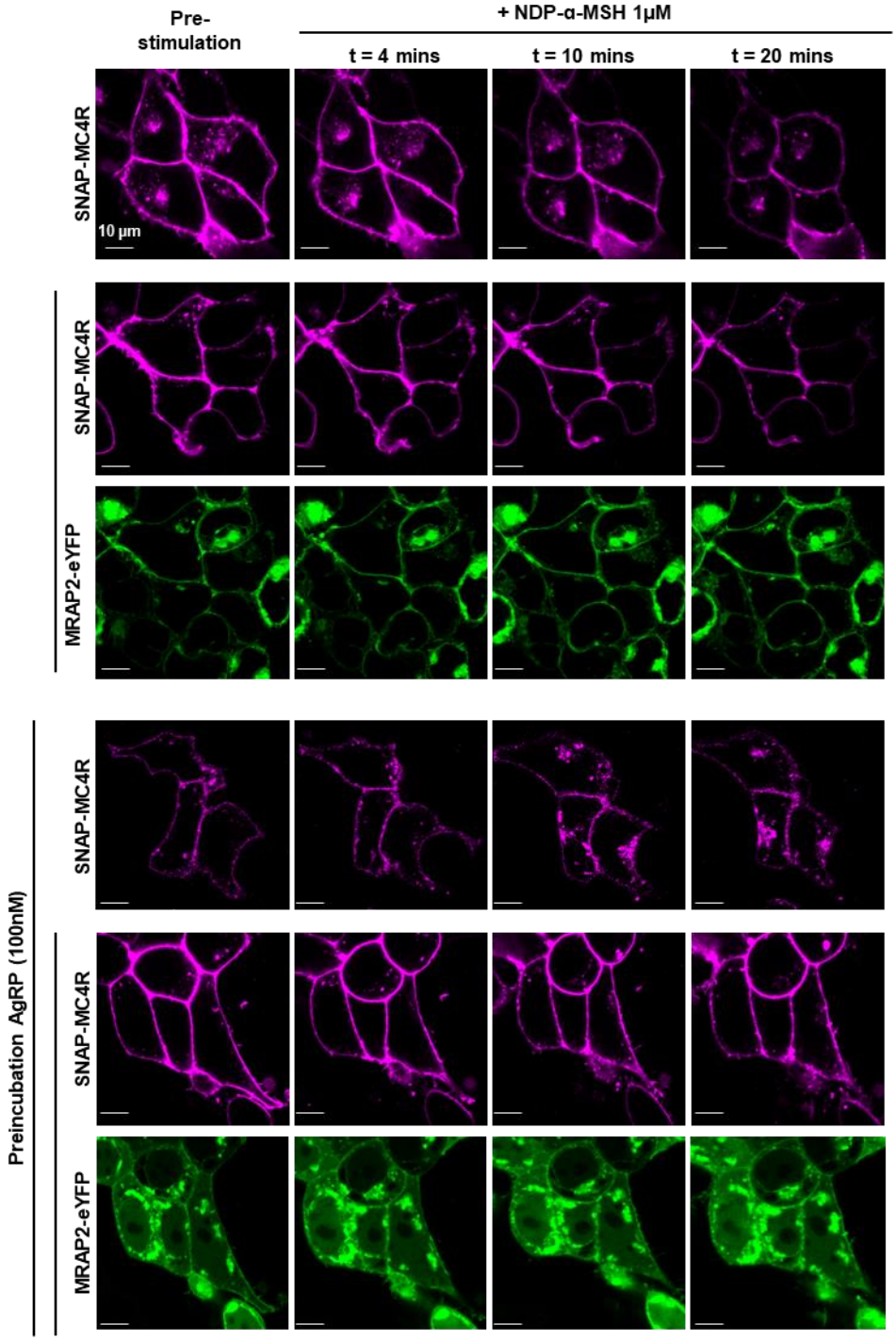

Supplementary Figure 6: Internalization of SNAP-MC4R with and without expression of MRAP2. From top to bottom, confocal micrographs of SNAP-MC4R together with eYFP-MRAP2, when indicated. Evolution of MC4R and MRAP2 cellular localization at four timepoints, before and respectively after 4, 10 and 20 minutes after the addition of 1μM NDP-α-MSH. In the right panel, cells expressing the receptor are further preincubated with 100 nM AgRP to suppress constitutive internalization.

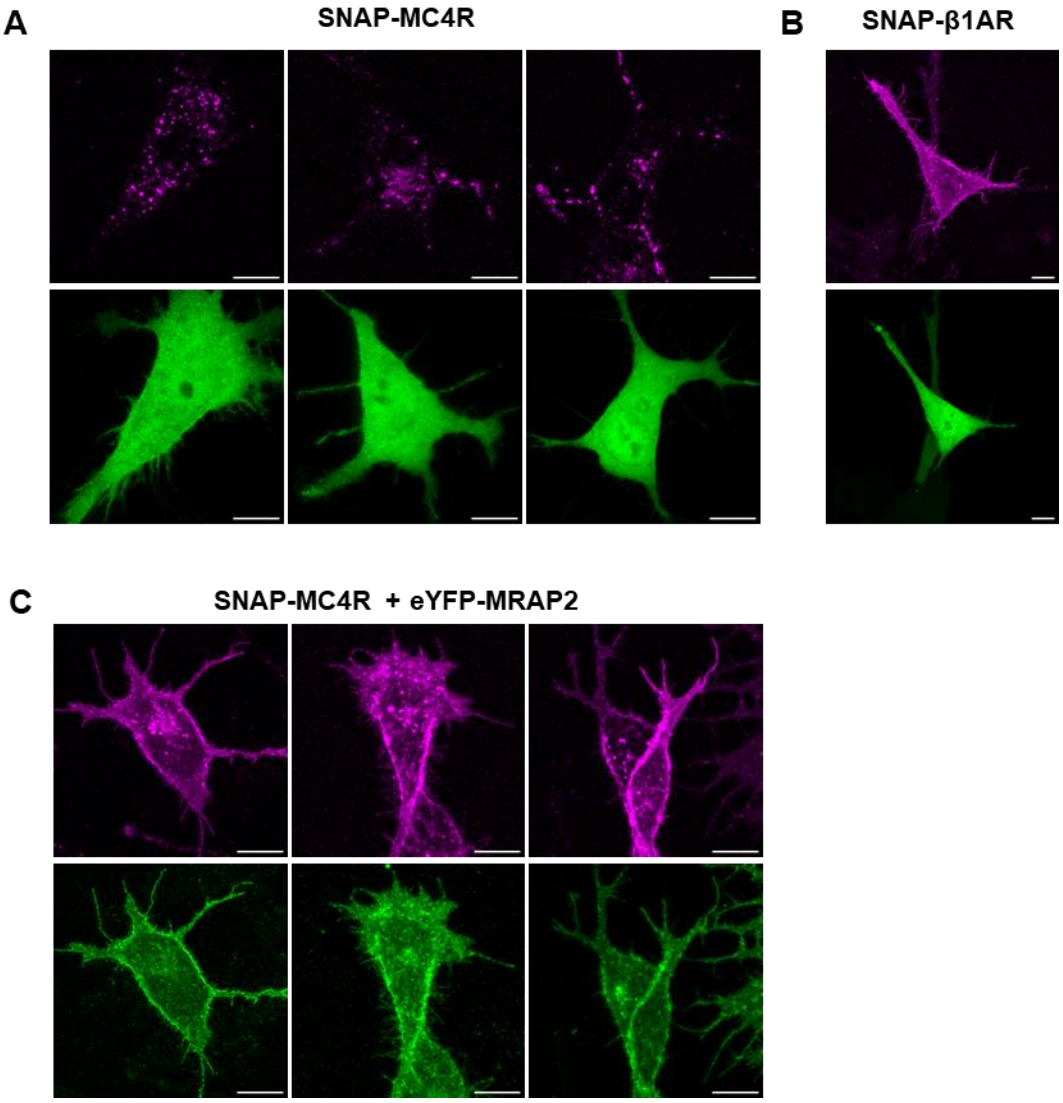

Supplementary Figure 7: Trafficking of SNAP-MC4R in the absence and presence of MRAP2 co-expression in N7 Embryonic Mouse Hypothalamus Cell. (A) Representative N7 cells electroporated with SNAP-MC4R and cytosolic GFP and further labeled with SNAP-Surface Alexa 647. **(B)** Representative N7 cells electroporated with SNAP-β1AR and cytosolic GFP and further labeled with SNAP-Surface Alexa 647. **(C)** Representative N7 cells electroporated with SNAP-MC4R and EYFP-MRAP2 and further labeled with SNAP-Surface Alexa 647. Confocal micrographs, scale bars are10 µm.

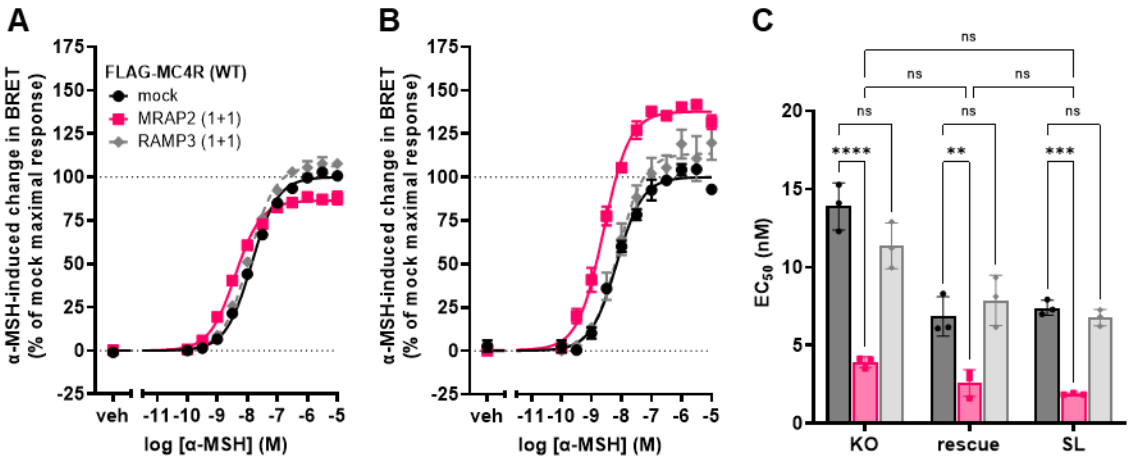

Supplementary Figure 8: MiniGs recruitment in β-arrestin1 and β-arrestin2 double knock-out cell. **(A)** Average concentration-response curves of Rluc8-miniGs recruitment to the plasma membrane localization sensor rGFP-CAAX upon MC4R stimulation with α-MSH for 45 minutes, in the presence or absence of MRAP2 or RAMP3, in transiently transfected β-arrestin1 and β-arrestin2 double knock-out cells. **(B)** β-arrestin1 and β-arrestin2 expression rescued the phenotype observed in related SL cells (not directly parental cells, as KO cells were maintained in FBS medium, while SL were maintained in NCS medium). Normalized data are expressed as mean ± SEM of three independent experiments. **(C)** EC_{50} values from the miniGs recruitment BRET experiments in double KO cells, in absence (KO) or presence of the reintroduction of β-arrestins (rescue), expressed as mean ± SEM of three independent experiments. EC_{50} in HEK293-SL cells from Figure 5D are rapported for comparison (SL). Statistical analysis was performed using two-way ANOVA with Turkey's multiple comparisons post-hoc test (*** = $p < 0.001$, **** = $p < 0.0001$).

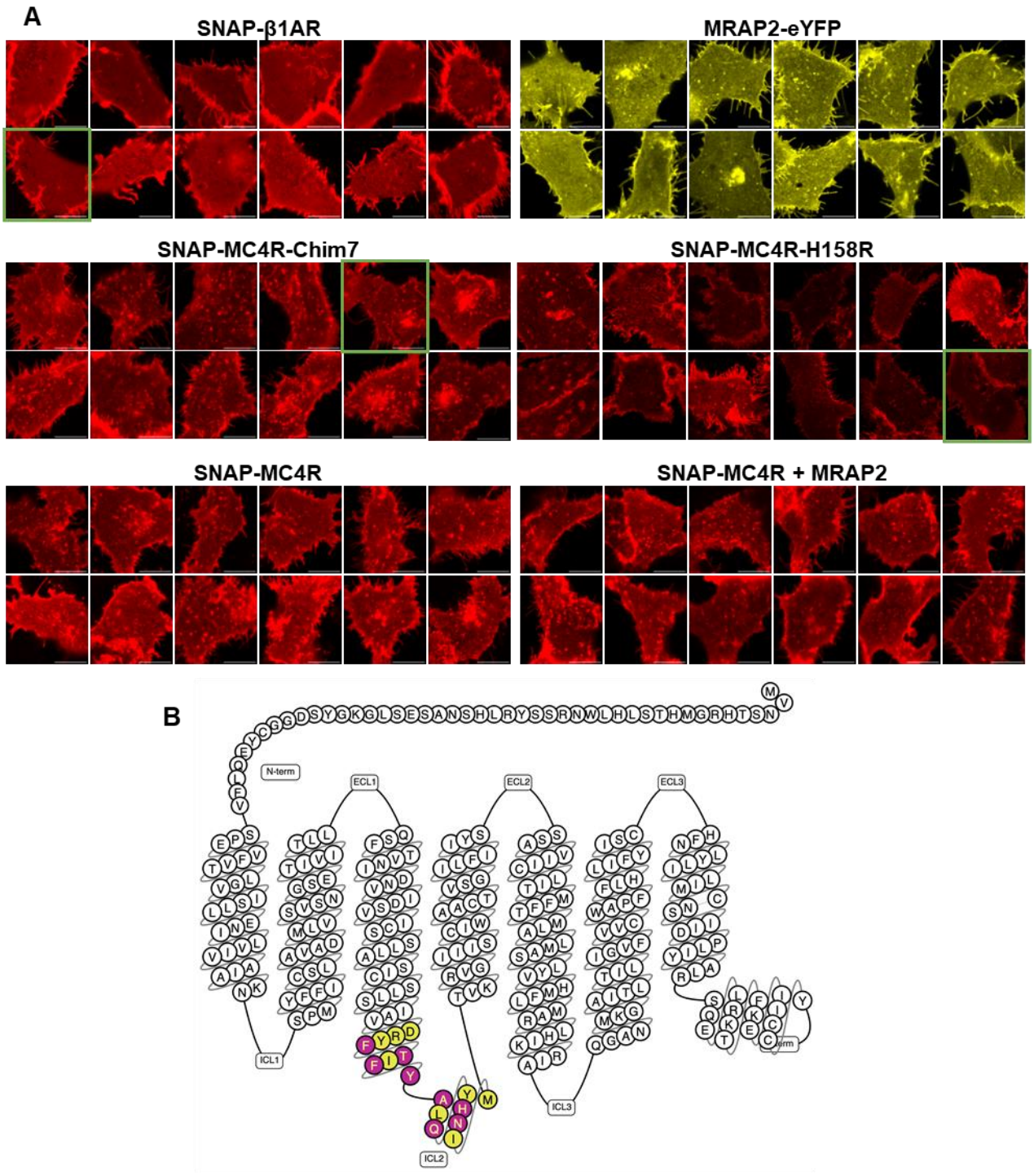

Supplementary Figure 9: Control datasets for molecular brightness experiments. (A) Representative confocal micrographs of HEK293 cells expressing the constructs used throughout the manuscript for fluorescence microscopy, all labeled with SNAP-surface Alexa 647. Green borders indicate the pictures that were used for Figure 6. **(B)** Snake plot diagram illustrating the mutated residues in ICL2 loops to generate MC4Rchim.

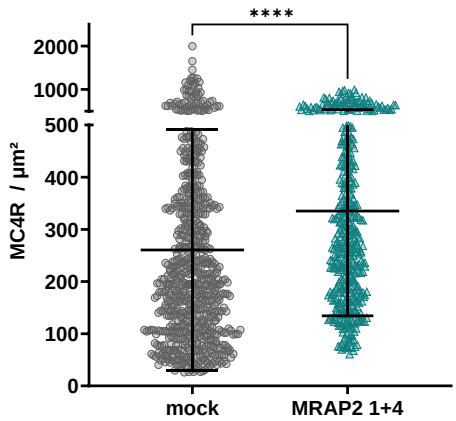

Supplementary Figure 10: Dependence of MC4R surface expression of MRAP2 expression levels. Measurements conducted using molecular brightness. Mean and SD are displayed on top of individual points reflecting molecular brightness from ROIs measured within individual cells. SNAP-MC4R (44 cells, 6 transfections) and SNAP-MC4R + MRAP2 (3 transfections, 15 cells).

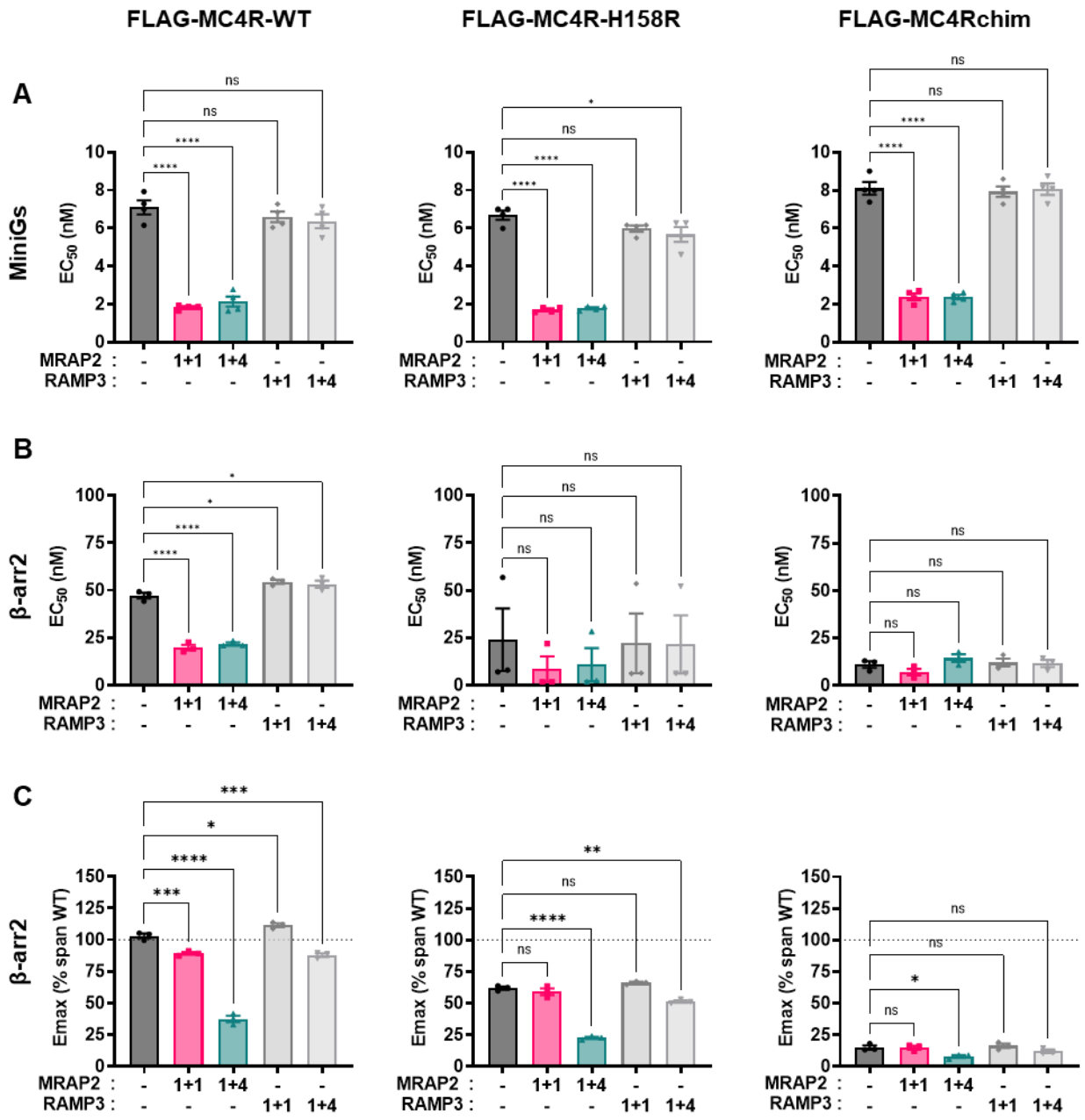

Supplementary Figure 11: Parameters for concentration-response curves of the MC4R-WT, MC4R-H158R and MC4Rchim in Figure 7. (A) EC_{50} values and **(B)** E_{max} values from the Rluc8-miniGs recruitment BRET experiments. Points represent average values across the four independent experiments, and mean and SEM are indicated. **(C)** E_{max} values from the β-arrestin2 recruitment BRET experiments. Points represent average E_{max} across the three independent experiments, and mean and SEM are indicated. Statistical analysis was performed using ordinary one-way ANOVA with Dunnett's multiple comparisons post-hoc test (* = $p < 0.05$; ** = $p < 0.01$, *** = $p < 0.001$; **** = $p < 0.0001$).

Supplementary Figure 12: Alignment of the human MRAP1 and MRAP2 sequences. This alignment was visualized using the software BioEdit(Hall 1999). Specific background colors reflecting physicochemical properties of the amino acid side chains: black - proline; blue - positively charged; cyan/green - aromatic and hydrophobic; green - hydrophobic; red - negatively charged; grey - hydrophilic; dark red - cysteines; and magenta – histidine. Of note, this (structural) alignment without gaps is different to recently supposed (Luo, Feng et al. 2023), where the MRAP1 '$_{18}$LDYL$_{21}$' motif is suggested to be an MRAP1 specific insertion (or is deleted in MRAP2) compared to the MRAP2 sequence.

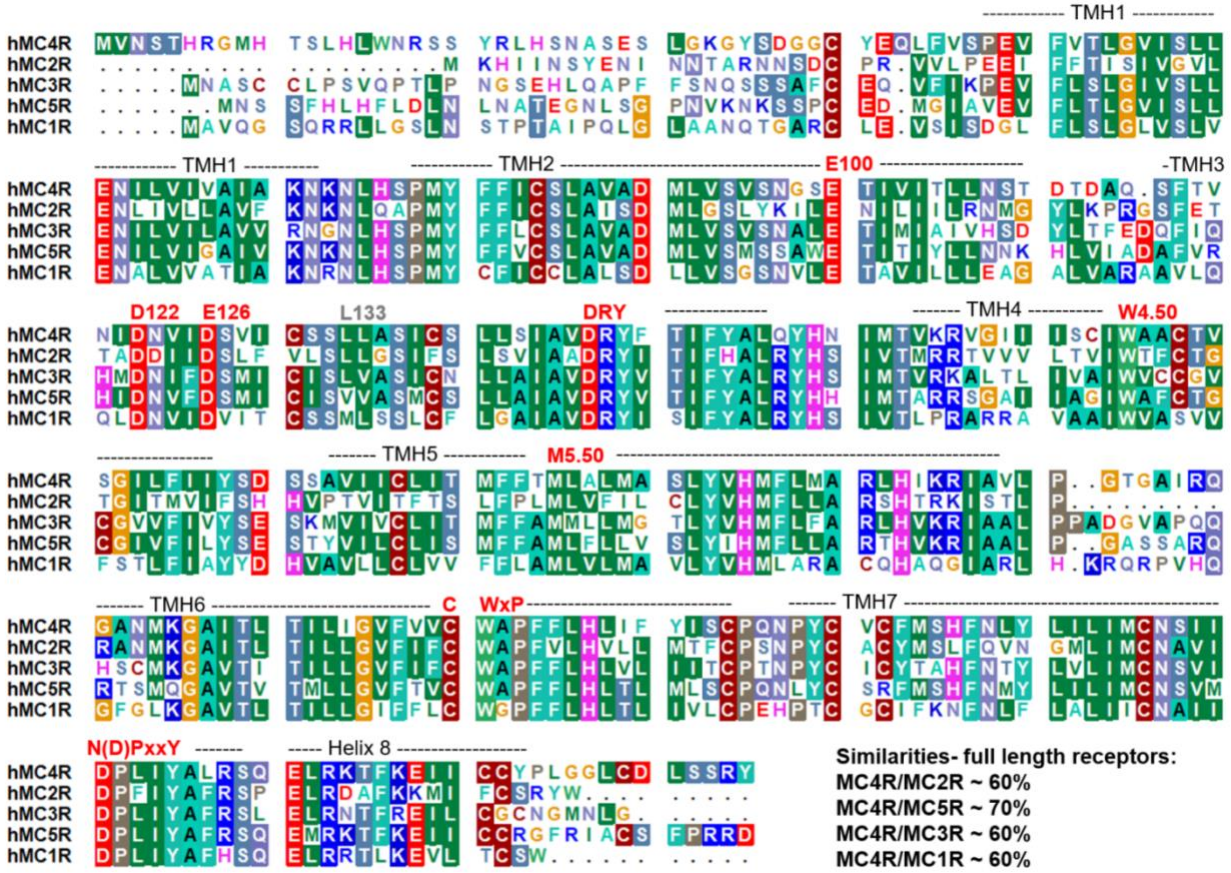

Supplementary Figure 13: Alignment of the human MCR sequences. This alignment was visualized using the software BioEdit(Hall 1999). Specific background colors reflecting physicochemical properties of the amino acid side chains: black - proline; blue - positively charged; cyan/green - aromatic and hydrophobic; green - hydrophobic; red - negatively charged; grey - hydrophilic; dark red - cysteines; and magenta – histidine. Additionally the structural lengths of helices as observed in the MC4R structures are indicated, as well as highly conserved amino acids. The negatively charged amino acids E100, D122 and D126 involved in calcium binding are also highlighted.

METHODS

Cell culture

Different variants of Human Embryonic Kidney cells (HEK293) were employed. HEK293T cell line (ECACC 96121229, Sigma-Aldrich) was used for plater reader and receptor localization and trafficking experiments. HEK293Adherent (HEK293AD) cell line (R70507, Thermo Fisher) was used for molecular brightness experiments (SpIDA). We refer to all three clones of HEK293 cells as HEK293 in the main text. Cells were grown in Dulbecco's Modified Eagle's Medium (DMEM, Pan Biotech), supplemented with 2 mM L-glutamine (Pan Biotech), 10 % (v:v) heat-inactivated Fetal Calf Serum (Biochrome), 100 µg/mL streptomycin, and 100 U/mL penicillin (Gibco) at 37 °C in a 5 % CO_2 incubator. HEK293 cells were grown in T75 cm^2 flasks. Upon reaching approximately 80 % confluency, cells were washed with 5 mL phosphate-buffered saline without Ca^{2+} and Mg^{2+} ions (DPBS, Sigma-Aldrich), trypsinised using 3 mL 0.05 % / 0.02 % trypsin/ethylenediaminetetraacetic acid solution (Pan Biotech) and passaged every 2 to 3 days. Cells were routinely tested for mycoplasma infection using MycoAlert Mycoplasma Detection Kit (Lonza). mHypoE-N7 cells (Cedarlanrelabs) were maintained in antibiotic-free DMEM/10 % FBS/2 mM L Ala-L-Gln at 37 ° C/ 5 % CO_2.

Seeding and transfection

25-mm glass coverslips and 96-well microtiter plates were coated with poly-D-lysine (PDL) (1 mg/ml) for 30 minutes, washed twice with PBS, and left to dry before seeding. For microscopy experiments, 3×10^5 cells were seeded on to clean and PDL-coated glass coverslips (Sigma-Aldrich) into a six-well plate, whereas cell seeding density of 40,000 cells per well was used for plate reader assays. After 24 h, cells were transfected with JetPrime, according to the manufacturer's protocol. For all transfections, MC4R:pcDNA3/MRAP2 ratio was 1:4, unless otherwise noted. The empty backbone of pcDNA3 as mock was used throughout to maintain a consistent level of total cDNA. Plasmid DNA constructs for hMC4R, MC4RChim and hMRAP2 were kindly provided by Prof. Heike Biebermann (Charite) and subcloned into pcDNA3 and pVITRO2 backbones using Gibson assembly with appropriate SNAP- and eYFP tags respectively. mHypoE-N7, an embryonic mouse hypothalamic cell line were transfected by electroporation using a Neon Transfection System (Invitrogen). One million cells were suspended with 7.5 µg total plasmid DNA, electroporated then seeded across three 25 mm-diameter polylysine-coated 1.5 thickness glass coverslips. SNAP-MC4R was co-transfected at a mass ratio of 1:4 with either EYFP-MRAP2 or pEGFP-N1. SNAP-β1-AR was co-transfected 1:4 with pEGFP-N1.

Transfection via Lipofectamine 3000

HEK293 cells were transiently transfected following the reverse transfection method using Lipofectamine™ 3000 (Thermo Fisher). Two transfection mixes (A & B) were prepared, in Mix A the DNA was diluted in 25 mL OptiMEM® media, and in Mix B 0.3 mL/well of P3000™ was added. In Mix B, 0.3 mL/well of Lipofectamine™ was added to 25 mL OptiMEM® media and each mix was incubated for 5 min. The DMEM in the HEK293 cells at approximately 70 % to 85 % confluency was removed and washed with DPBS without Ca^{2+} and Mg^{2+}, trypsinised and centrifuged as described above. Meanwhile, Mix A containing the DNA was added to Mix B containing Lipofectamine™ mix dropwise and incubated for 15 min at room temperature. The cell pellet was resuspended in 10 mL DMEM-High Glucose media, counted and diluted at a density of 75,000 cells/well. 50 µL of the transfection mix was added into a poly-D-lysine (Sigma-Aldrich) coated clear white F-bottom 96-well plate followed by 100 mL of the cell suspension. The plate was incubated at 37 °C in a 5 % CO_2 incubator for 24 h.

Epac-S^{H187} FRET-sensor based cAMP assay

HEK293T cells were seeded into 10 cm Petri dishes (3.5x10^6 cells) and after 24 h transfected with the combination of Epac-S^{H187} FRET biosensor, pcDNA3, SNAP-MC4R and Epac-S^{H187} biosensor, SNAP-MC4R and MRAP2. Plasmid DNA combinations were transfected at a ratio of 5:1:1 or 5:1:4 respectively. Media was changed 4 h after transfection. Twenty-four hours post-transfection, cells were re-seeded into PDL-coated black-wall, black bottom 96-well plates at a density of 40,000 cells per well. 36 h after transfection, cells were washed, and medium was changed to HBSS buffer supplemented with 0.1 % BSA. Plate reader experiments were performed using a Synergy Neo2 plate reader (BioTek) equipped with a monochromator and filter optics. Expression levels of receptor, biosensor and accessory protein were measured with monochromator optics. For expression of MC4R and MRAP2, cells were excited at 558/20 nm and fluorescence emission was recorded at 605/20 nm while for biosensor the excitation was at 500/20 nm, and emission was at 539/20 nm. For FRET measurements, a range of CFP/YFP monochromators were used, which was excited at 430/20 nm, while 491/30 nm and 541/20 nm were used for emission.

In 90 µL HBSS buffer, acceptor baseline fluorescence was measured. Then, pre-stimulation basal reads for 5 minutes were recorded. Afterwards, 10 µL of 10-fold ligand solution was applied to each well and the post-stimulation reads were recorded for a further 25 min. Subsequently, Forskolin/IBMX was added to each well to record maximal stimulation reads.

cAMP signaling assay with Glo sensor

The transfection mix was prepared, in Mix A, 50 ng/well of pGloSensor™-22F cAMP sensor plasmid (Promega), 50 ng/well of the 3x HA MC4R plasmid and 50 ng/well pcDNA3.1 or MRAP2-FLAG were added to 25 mL/well OptiMEM® media. To this, 0.3 mL/well of P3000™ was added. In Mix B, 0.3 mL/well of Lipofectamine™ was added to 25 mL OptiMEM®. 24 h after transfection via lipofectamine, the cell culture media was removed and the cells were washed with cAMP assay buffer (1x HBSS, 24 mM HEPES, 0.1 % (*w:v*) BSA, 3.96 mM $NaHCO_3$, 1 mM $MgSO_4$, 1.3 mM $CaCl_2$ ($2H_2O$), pH 7.4). The plate was then equilibrated for 1 hour at 28 °C with 70-90 mL of cAMP buffer supplemented with 0.45 mg/mL of Firefly D-Luciferin free acid (NanoLight Technology). If Dynasore (HelloBio) is incorporated into the experiment an additional step is taken, whereby post equilibration, 20 µL of Dynasore (80 µM/well) is added to each well and incubated for 15 min at room temperature. Thereafter, the basal readings are performed on the CLARIOstar® Plus Plate Reader (BMG LabTech, Germany) and the relative luminescence units (RLU) were measured for approximately 5 minutes before stimulating the cells with 10 µL of agonist, vehicle or forskolin. The final volume in each well was 100 µL. An average of the basal reads was used to normalize the response of each well. Bioluminescence was measured for a total of 66 cycles (1 min per cycle), with a 1-second integration time and no lens.

Nanobody recruitment assay

HEK293AD cells were seeded in PDL-coated 8-well Ibidi slides at a density of 25000 cells per well, following with JetPrime transfection the next day, according to the manufacturer's protocol. Plasmid DNA ratios used for co-transfection were as follows: for Nb35/37 recruitment, 1x SNAP-MC4R+4x pcDNAmock/MRAP2, 1x Nb35-eYFP/Nb37-eYFP and 3x Gs (tricistronic). Next day, transfected cells were labeled with SNAP-Surface Alexa Fluor 647 dye (NEB) as described earlier. Afterwards, cells were subsequently taken for imaging to an Attofluor Cell Chamber (Fisher Scientific, GmbH) in 1x HBSS supplemented with 0.1 % BSA. A TIRF illuminated Eclipse Ti2 microscope (Nikon), equipped with a 100X, 1.49 NA automated correction collar objective, and with 405, 488, 561, and 647 nm laser diodes coupled via an automated N-Storm module and four iXon Ultra 897 EMCCD cameras (Andor), was used. During imaging, both the cell imaging chamber holding Ibidi slide, and objectives were kept at 37 °C. The automated objective collar was kept on and hardware autofocus was activated.

The acquisition of movies was performed at 4 seconds per frame for 400 frames. Initially, a baseline measurement of 25 frames was done and then NDP-α-MSH was added at a concentration of 1 µM to the well. Fluorescence intensity values were extracted by employing ImageJ. Background correction and normalization was made for pre-stimulation and post-stimulation.

IP_1 accumulation assay

Cellular IP1 as a readout for Gq signaling was measured using a commercial HTRF competitive immunoassay (IP-One Gq kit, CisBio) as described in the manufacturer's protocol. For this purpose, HEK293T cells were seeded into 10 cm Petri dishes ($3.5x10^6$ cells) and after 24 h transfected with the combination of plasmids (pcDNA3+SNAP-MC4R) and (SNAP-MC4R+MRAP2) at a ratio of 1:4, using JetPrime according to the manufacturer's protocol. Media was changed 4 h after transfection. Twenty-four hours post-transfection, 20 µL of cell suspension at a density of 15,000 cells per well was re-seeded into opaque white flat-bottom 384-well plates (Corning) and left to equilibrate for 2 hours at 37 °C in a 5 % CO2 incubator. Afterwards, the cells were stimulated with ligand concentrations (dilution series for concentration response curve) prepared in stimulation buffer (HBSS supplemented with 20mM LiCl) for 2 hours under cell culture conditions. Following incubation, the FRET acceptor (IP_1-d2) and the FRET donor (anti-IP_1-Cryptate antibody) were reconstituted and diluted in lysis and detection buffer as described in the manufacturer's protocol. 3 µL each of both solutions was added per well separately in the order described, and the plate was incubated on a shaker for an hour at room temperature. Fluorescence emission was detected at 620 nm and 665 nm at the plate reader (Synergy Neo2 plate reader, BioTek). The HTRF ratio was calculated by dividing the detected emission at 665 nm by the detected emission at 620 nm. The EC_{50} values were calculated using the GraphPad Prism 10 software (GraphPad Software, San Diego, CA, USA).

NFAT reporter assay

HEK293 cells were transfected 24 hours after seeding. For determination of phospholipase C (PLC) activation (read-out for Gq/11 signaling) via nuclear factor of activated T-cells (NFAT) reporter gene assay, cells were transfected with 45 ng plasmid-DNA, 0.45 µl Metafectene (Biontex, Munich, Germany) and with 45 ng NFAT reporter DNA per well in MEM without supplements.

For PLC activation, the NFAT responsive element (NFAT-luc, pGL4.33) was co-transfected with the plasmids for MC4R and MRAP2 in a ratio of 1+1 (1:1) or 1+4 (1:4). 48h post transfection, cells were challenged with α-MSH (10 mM to 1 nM) in MEM without supplements for 4 h at 37 °C and 5 % CO_2. The stimulation was stopped by discarding the media and cell lysis was induced by the addition of 1x passive lysis buffer (PLB, Promega) and horizontal shaking for 15 min at room temperature.

For measurement of luciferase activity, 10 µl lysate were transferred into a white opaque 96 well plate. Injection of 40 µl firefly luciferase substrate (Promega) and measurement of luminescence was performed with a plate reader (Viktor Nivo, Perkin Elmer).

SNAP Tag labeling

Prior to microscopy imaging experiments, coverslips with cells (either HEK293 or mHypoE-N7) expressing SNAP-MC4R and MRAP2 were labeled with 1 µM SNAP-Surface Alexa Fluor 647 dye or SNAP-Surface Alexa Fluor 549 in complete DMEM (Pan Biotech) for 25 min and kept in the incubator at 37 °C and 5 % CO_2. Excessive dye was washed by exchanging with fresh medium with an interval of 5 minutes each for three times.

Time-lapse imaging with confocal microscopy

HEK293T cells ($3x10^5$ cell per well) were seeded on 25 mm glass coverslips in a 6-well plate, which were pre-coated with PDL. After 24 hours, cells were transfected with 2.5 µg DNA in total of SNAP-MC4R and MRAP2 constructs (1:4 ratio) using JetPrime according to the manufacturer's protocol. Media was exchanged to fresh media 4 hours after transfection. Next day, transfected cells were labeled with SNAP-Surface Alexa Fluor 647 dye. Afterwards, coverslip with labeled cells was placed in the Attofluor cell chamber (Thermo Fisher Scientific) with 450 µL of the imaging buffer (HBSS supplemented with 0.1 % BSA) and the chamber was placed in the placeholder for image acquisition. Pre-stimulation images were taken for the first 3-5 minutes and then 50 µL of agonist NDP-α-MSH was carefully added on top of cells to the final concentration of 1µM in the chamber and image acquisition was performed for 30 min post-stimulation.

Imaging was performed using Leica SP8 confocal microscope system with 40x/1.25 NA oil immersion objective, a photon counting hybrid detectors and a white light laser (WLL). 488 and 633 nm lines of the WLL were used for excitation and emission bands of 520 nm to 600 nm and 650 nm to 730 nm were used for detection of eYFP and SNAP-Surface Alexa 647, respectively. Imaging format was xyt, and image size was set to 1024×1024 pixels and 100 Hz scan speed. Image analysis was performed using ImageJ.

For mHypoE-N7 and HEK293 used in Supplementary Figure 4 multitrack confocal z stacks were acquired on a Zeiss LSM800 Airyscan microscope using a 63× 1.4 NA objective at 50 nm lateral pixel resolution. Laser excitation/emission collection (nm) was 488/500-550 for EGFP/EYFP, 561/580-630 for SNAP surface 549 and 640/650-700 for AF647. Maximum intensity projections were constructed in FIJI and all images are presented on a common intensity scale.

NanoBiT arrestin recruitment assay

HEK293 cells (75,000 cells/well) were seeded in white bottom 96-well plate and reverse co-transfected with Lipofectamine 3000, whereby the plasmid encoding the MC4R-LgBiT (50 ng/well) and the SmBiT-β-arrestin 2 (10 ng/well) were used. 24 h post-transfection, the cells were rinsed once with assay buffer (1X HBSS, 24 mM HEPES, 0.1% (*w:v*) BSA, 3.96 mM $NaHCO_3$, 1 mM $MgSO_4$, 1.3 mM $CaCl_2$ ($2H_2O$), pH 7.4) and the plates were pre-equilibrated in the dark for 1h at 37 °C with 90 µL of assay buffer. Post-equilibration, 25 µL/well of a 5x solution of the Nano-Glo® Live cell reagent (NanoLight Technology) was added, and luminescence readings were taken every minute at 37 °C until the signal was stable (3-5 min), representing the basal activity. Immediately after, 10 µL of agonist/vehicle were added and luminescence was further recorded for 60 min (no lens, 0.5 s integration time and 1 min intervals at 37 °C using a CLARIOstar® Plus Multimode Plate Reader (BMG Labtech, Germany). The final volume in each well was 125 µL. To account for differences in expression/cell density, the average of at least 3 stable pre-readings was used to normalize each well response before proceeding with further analysis using the area under the curve parameter.

Molecular brightness analysis with SpIDA

HEK293AD cells (3×10^5 cells/well) were seeded on clean glass coverslips in six-well plates and were transfected with MC4R and MRAP2 constructs for overnight using JetPrime as a transfection reagent according to the manufacturer's protocol. For SNAP-tag incorporated receptors, labeling was performed as described above using SNAP-Surface Alexa Fluor 647 dye. Coverslips with transfected cells were placed in an Attofluor cell chamber (Thermo Fisher Scientific) and supplemented with Flourobrite DMEM supplemented with 2 mM L-glutamine (Pan Biotech), 10% fetal calf serum (Biochrome), 100 µg/mL streptomycin, and 100 U/mL penicillin (Gibco).

SpIDA imaging was performed using a commercial laser-scanning confocal microscope (Leica SP8) equipped with a 40×/1.25 NA oil immersion objective, a white light laser (WLL), and photon counting hybrid detectors; 514 and 633 nm lines of the WLL were used for excitation, and emission bands of 520 nm to 600 nm and 650 nm to 730 nm were used for detection of eYFP and SNAP-Surface Alexa 647, respectively. Imaging format was xy, and image size was set to 512 × 512 pixels with 50 nm pixel size and 100Hz scan speed. Image analysis was performed using ImageJ. Polygonal region of interest (ROI) selection was implemented and areas with inhomogeneous fluorescence distribution were avoided.

Homology modeling of MC4R–MRAP2 complex

A structural homology model of an agonist–MC4R–MRAP2–Gs complex was designed based on the recently determined ACTH–MC2R–MRAP1–Gs complex (PDB ID: 8gy7)(Luo, Feng et al. 2023) and the NDP-α-MSH–MC4R–Gs protein complex (PDB ID: 7piv)(Heyder, Kleinau et al. 2021) as structural templates. Both MC2R-MC4R as well as MRAP1-MRAP2 share high sequence similarities of ~60%, respectively (N-terminal and transmembrane helix sequences of MRAP1 with MRAP2 that are relevant for modeling were compared) (**Supplementary Figures 11** and **12**). This high similarity supports the idea of potential homology between the two receptor-MRAP complexes, however, differences in detail must be considered especially with respect to ligand binding modes. The complexes were superimposed at the receptors transmembrane region, and MRAP was merged from the ACTH–MC2R–MRAP1–Gs complex into the high resolution (2.58 Å) NDP-α-MSH–MC4R–Gs protein complex. NDP-α-MSH was substituted by α-MSH as known from the α-MSH–MC4R complex(Zhang, Chen et al. 2021), with a lower resolution of ~3 Å. The sequence of MRAP1 was substituted by corresponding amino acid residues of MRAP2. Of note, the used alignment between MRAP1 and MRAP2 sequences is without gaps (Suppl. Fig. 9) and is, therefore, different to a recently supposed(Luo, Feng et al. 2023). The N-terminal MRAP1 '$_{18}$LDYL$_{21}$' motif is suggested to be an MRAP1 specific feature compared to the MRAP2 sequence, and is significant to mediate the effect of increased ACTH action at MC2R. This might be different to (structurally unknown) MC4R-MRAP2-ACTH complexes, whereby it was already shown that co-expressed MRAP2(Josep Agulleiro, Cortes et al. 2013, Soletto, Hernandez-Balfago et al. 2019) increases ACTH binding and signaling to a high extent, in contrast to α-MSH. In MRAP2 the exact MRAP1 '$_{18}$LDYL$_{21}$' motif is missing or is potentially structurally substituted by a '$_{25}$YEYY$_{28}$' motif with similarities as considered in the alignment presented in Suppl. Fig. 9. For all steps of structural modifications, the software SYBYL-X 2.0 (Certara, NJ, US) was used and the initial complex model was optimized by energy minimization with the Amber99 force field until converging at a termination gradient of 0.05 kcal/(mol*Å) under constrained backbone atoms. Side chain orientations were optimized by a 2 ns molecular dynamics simulation (MD) with constraint backbone atoms. Finally, the entire complex model α-MSH–MC4R–MRAP2–Gs was energetically minimized without any constraint.

BRET-based assays

HEK293-SL cells(Namkung, Le Gouill et al. 2016), a subclone of Ad5-transformed HEK293 cells kindly given by S. Laporte (McGill University, Montreal, Canada), were cultured in DMEM (Wisent Bioproducts) supplemented with 10% newborn calf serum (Wisent Bioproducts). β-arrestin1 and β-arrestin2 double knock-out cells, generated by CRISPR technology from HEK293-SL cells(Moller, Pedersen et al. 2020), were cultured in DMEM (Wisent Bioproducts) supplemented with 10% fetal bovine serum (Wisent Bioproducts). Both cell lines were cultured with additional 100 UI/mL penicillin and 100 µg/mL streptomycin (Wisent Bioproducts) in an incubator set to 37°C and 5% CO_2. Cells were routinely tested for mycoplasma infection using PCR Mycoplasma Detection Kit (ABM#G238).

The day of the transfection, cells are distributed 100 uL per well at a density of 350,000 cells/mL in Cellstar© opaque white 96-well plates (Greiner Bio-One) with 1 µg/mL of total plasmid DNA and 3 µg/mL of 25 kDA linear polyethyleneimine (Alfa Aesar). Plasmids encoding for Rluc8-C1_Rluc8-miniGs(Avet, Mancini et al. 2022), pcDNA3.1hygro(+)_p63RhoGEF-RlucII, pcDNA3.1hygro(+)_Rap1GAP-RlucII(Avet, Mancini et al. 2022), pcDNA3.1hygro(+)_β-arrestin2-RlucII, pcDNA3.1(+)_rGFP-CAAX, pcDNA3.1(+)_rGFP-FYVE (Namkung, Le Gouill et al. 2016) , pcDNA3.1(+) MRAP2, (Kay, Botha et al. 2013) and β-arrestin1 and β-arrestin2 were already described. RAMP1 and RAMP3 were kindly provided by S. M. Foord (GlaxoSmithKline) and subcloned into pcDNA3 as previously described(Heroux, Breton et al. 2007). pcDNA3.1_$G\alpha_q$ and pcDNA3.1_$G\alpha_{15}$ were purchased from cDNA Resource Center. New pcDNA.3.1(+)_MC4R-RlucII was generated from 3xHA-hMC4R-RlucII using Gibson assembly to remove the N-terminal 3xHA tag, and to add a full Kozak consensus sequence before the receptor, to revert the silent mutation c.G993A to refseq sequence, and to replace the linker with GGGGSKLPAT between the human MC4R (MCR040TN00, cDNA Resource Center) and the RlucII(Namkung, Le Gouill et al. 2016). For the BRET assays, either SNAP-MC4R or FLAG-MC4R were used respectively for MC4R-WT evaluation or MC4R-H158R and MC4Rchim evaluation. The SNAP-MC4R is in a pVITRO2 dual expression vector (Invivogen), in which mRuby2 is expressed under the FerL promoter, and the SNAP-MC4R is expressed under the FerH promoter. The SNAP-MC4R is N-terminally tagged with consecutively an Ig kappa ladder signal peptide (Igκ), a hemagglutinin A (HA) tag, a Strep-Tag®II (ST) tag and a SNAP-tag® (Igκ-HA-ST-SNAP-MC4R). The FLAG-MC4R is in a pcDNA3.1(+) expression vector (Invitrogen) and was previously described(Farooqi, Yeo et al. 2000). Cloning for H158R was performed using Q5 mutagenesis with forward primer TCTCCAGTACcgcAACATTATGAC and reverse primer GCATAGAAGATAGTAAAGTAC on pcDNA3.1(+)_FLAG-hMC4R(WT) template. Cloning for Chim7 was performed using forward primer agctggctagcgtttaaacttaagcttgccaccATGGATTACAAGGATGACGACGATAAGggtaccATGGTGAACTCCACCCACC and reverse primer tcagcgggtttaaacgggccctctagaggctcaTTAATATCTGCTAGACAAGTCACAAAGGCC on pcDNA3_SNAP-Chim7 template previously described.

Total plasmid transfected was adjusted to 1000 ng with pcDNA3.1(+) and fixed plasmid amounts were as follows: 25 ng MC4R-RlucII, 400 ng rGFP-FYVE, 300 ng rGFP-CAAX, 5 ng p63RhoGEF-RlucII with 100 ng $G\alpha_q$, 10 ng p63RhoGEF with 50 ng $G\alpha_{15}$, 5 ng β-arrestin2-RlucII, 5 ng Rluc8-miniGs. For β-arrestins rescue experiments, both β-arrestins were reintroduced at 100 ng each. MC4R amounts were adjusted to be around the middle of the linear range of each functional assays, which is 100 ng for miniGs recruitment assay, 140 ng for β-arrestin recruitment assay, 400 ng for p63RhoGEF recruitment assay with $G\alpha_q$, 10 ng for p63RhoGEF recruitment assay with $G\alpha_{15}$. MRAP2 amounts were used at varying amounts, but RAMP3 amounts were only tested at the higher of the MC4R:MRAP2 ratio used for some assays.

Two days after transfection, plates were washed with PBS supplemented with 1 mM $CaCl_2$ and 1

mM $MgCl_2$ (PBS+CM), and equilibrated at 37°C for approximately 1h in Tyrode HEPES buffer (NaCl 137 mM, $MgCl_2$ 1 mM, $NaHCO_3$ 11.9 mM, NaH_2PO_4 3.6 mM, KCl 0.9 mM, glucose 5.5 mM, $CaCl_2$ 1 mM, with pH adjusted to 7.4 with NaOH). Total fluorescence of the rGFP ($\lambda_{excitation}$ 485 nm, $\lambda_{emission}$ 538 nm, auto cutoff 530 nm) and/or the mRuby2 ($\lambda_{excitation}$ 550 nm, $\lambda_{emission}$ 615 nm, cutoff set to 610 nm) was red before BRET experiments using FLEX station II (Molecular Devices), respectively to control for plasmid competition of the biosensors and dual expression of the pVITRO2_SNAP-MC4R.

For dose-response curve experiments, cells were incubated with increasing concentrations of α-MSH (GenScript) with 0.01% m/V bovine serum albumin (Biobasic) for 45 minutes for G protein activation assays, for 2 or 3 minutes for β-arrestin2 recruitment assay and for 60 minutes for internalization assay. Prolume Purple methoxy e-Coelenterazine (NanoLight Technology) was added 10 minutes before reading (1 µM final). Light measurements at 410/80 nm (donor) and 515/20 nm (acceptor) channels were integrated for 0.1 second at 37°C on Tristar² LB942 (Berthold Technology). BRET is calculated as the ratio of the light emitted in the acceptor channel over the light emitted in the donor channel.

Results were normalized to the α-MSH-induced change in BRET ratio of the mock condition.

$$\text{α-MSH-induced change in BRET (\%)} = \frac{\text{BRET}_{\text{condition}} - \text{bottom asymptote}_{\text{condition}}}{\text{span}_{\text{mock}}} * 100$$

Concentration-response curves and parameters, such as bottom asymptote, span and $\log EC_{50}$ were calculated by GraphPad Prism using 3-parameters non-linear regression. E_{max} is calculated manually as span ratio over the mock. It is to note that all calculations excluded changes in basal.

$$E_{max}\ (\%) = \frac{\text{span}_{\text{condition}}}{\text{span}_{\text{mock}}} * 100$$

Statistical analysis were performed on GraphPad Prism (10.3.1).

sCFP3A-EPAC-Venus cAMP FRET assay

HEK293-SL cells were cultured and transfected like for the BRET experiments with 1000 ng of pcDNA3.1_sCFP3A-EPAC1(δDET+T781A+F782A)-venus and increasing amount of either pcDNA3.1(+)_MC4R-WT , pcDNA3.1(+)_FLAG-MC4R-WT or pcDNA3.1(+)_MC4R-WT-RlucII up to 200 ng, total DNA being maintained to 1200 ng with pcDNA3.1(+) empty vector.

Method to generate pcDNA3.1_sCFP3A-EPAC1(δDET+T781A+F782A)-venus was previously described(van der Westhuizen, Breton et al. 2014).

Two days after transfection, cells were washed with PBS+CM and equilibrated for 30 minutes in THB. Cells were incubated with increasing concentrations of α-MSH (GenScript) with 0.01% m/V bovine serum albumin (Biobasic) for 25 minutes. Fluorescence signals at 485/20 nm and 535/25 nm were read on Spark microplate reader (Tecan) with excitation at 430/20 nm. FRET values were calculated as light emitted in the 485 nm channel divided by sum of the light emitted in both 485 nm and 535 nm channels. Baseline-corrected values (representing the α-MSH-induced change in FRET) were calculated by substracting the bottom asymptote calculated by GraphPadPrism (10.3.1) for each independent experiment.

REFERENCES

Asai, M., S. Ramachandrappa, M. Joachim, Y. Shen, R. Zhang, N. Nuthalapati, V. Ramanathan, D. E. Strochlic, P. Ferket, K. Linhart, C. Ho, T. V. Novoselova, S. Garg, M. Ridderstrale, C. Marcus, J. N. Hirschhorn, J. M. Keogh, S. O'Rahilly, L. F. Chan, A. J. Clark, I. S. Farooqi and J. A. Majzoub (2013). "Loss of function of the melanocortin 2 receptor accessory protein 2 is associated with mammalian obesity." Science **341**(6143): 275-278.

Avet, C., A. Mancini, B. Breton, C. Le Gouill, A. S. Hauser, C. Normand, H. Kobayashi, F. Gross, M. Hogue, V. Lukasheva, S. St-Onge, M. Carrier, M. Heroux, S. Morissette, E. B. Fauman, J. P. Fortin, S. Schann, X. Leroy, D. E. Gloriam and M. Bouvier (2022). "Effector membrane translocation biosensors reveal G protein and betaarrestin coupling profiles of 100 therapeutically relevant GPCRs." Elife **11**.

Baron, M., J. Maillet, M. Huyvaert, A. Dechaume, R. Boutry, H. Loiselle, E. Durand, B. Toussaint, E. Vaillant, J. Philippe, J. Thomas, A. Ghulam, S. Franc, G. Charpentier, J. M. Borys, C. Levy-Marchal, M. Tauber, R. Scharfmann, J. Weill, C. Aubert, J. Kerr-Conte, F. Pattou, R. Roussel, B. Balkau, M. Marre, M. Boissel, M. Derhourhi, S. Gaget, M. Canouil, P. Froguel and A. Bonnefond (2019). "Loss-of-function mutations in MRAP2 are pathogenic in hyperphagic obesity with hyperglycemia and hypertension." Nat Med **25**(11): 1733-1738.

Bernard, A., I. Ojeda Naharros, X. Yue, F. Mifsud, A. Blake, F. Bourgain-Guglielmetti, J. Ciprin, S. Zhang, E. McDaid, K. Kim, M. V. Nachury, J. F. Reiter and C. Vaisse (2023). "MRAP2 regulates energy homeostasis by promoting primary cilia localization of MC4R." JCI Insight **8**(2).

Brouwers, B., E. M. de Oliveira, M. Marti-Solano, F. B. F. Monteiro, S. A. Laurin, J. M. Keogh, E. Henning, R. Bounds, C. A. Daly, S. Houston, V. Ayinampudi, N. Wasiluk, D. Clarke, B. Plouffe, M. Bouvier, M. M. Babu, I. S. Farooqi and J. Mokrosinski (2021). "Human MC4R variants affect endocytosis, trafficking and dimerization revealing multiple cellular mechanisms involved in weight regulation." Cell Rep **34**(12): 108862.

Bruschetta, G., J. D. Kim, S. Diano and L. F. Chan (2018). "Overexpression of melanocortin 2 receptor accessory protein 2 (MRAP2) in adult paraventricular MC4R neurons regulates energy intake and expenditure." Mol Metab **18**: 79-87.

Buch, T. R., D. Heling, E. Damm, T. Gudermann and A. Breit (2009). "Pertussis toxin-sensitive signaling of melanocortin-4 receptors in hypothalamic GT1-7 cells defines agouti-related protein as a biased agonist." J Biol Chem **284**(39): 26411-26420.

Cai, Z., O. F. Christensen, M. S. Lund, T. Ostersen and G. Sahana (2022). "Large-scale association study on daily weight gain in pigs reveals overlap of genetic factors for growth in humans." BMC Genomics **23**(1): 133.

Chan, L. F., T. R. Webb, T. T. Chung, E. Meimaridou, S. N. Cooray, L. Guasti, J. P. Chapple, M. Egertova, M. R. Elphick, M. E. Cheetham, L. A. Metherell and A. J. Clark (2009). "MRAP and MRAP2 are bidirectional regulators of the melanocortin receptor family." Proc Natl Acad Sci U S A **106**(15): 6146-6151.

Clement, K., H. Biebermann, I. S. Farooqi, L. Van der Ploeg, B. Wolters, C. Poitou, L. Puder, F. Fiedorek, K. Gottesdiener, G. Kleinau, N. Heyder, P. Scheerer, U. Blume-Peytavi, I. Jahnke, S. Sharma, J. Mokrosinski, S. Wiegand, A. Muller, K. Weiss, K. Mai, J. Spranger, A. Gruters, O. Blankenstein, H. Krude and P. Kuhnen (2018). "MC4R agonism promotes durable weight loss in patients with leptin receptor deficiency." Nat Med **24**(5): 551-555.

Elsner, A., P. Tarnow, M. Schaefer, P. Ambrugger, H. Krude, A. Gruters and H. Biebermann (2006). "MC4R oligomerizes independently of extracellular cysteine residues." Peptides **27**(2): 372-379.

Fan, S., H. Liu and L. Li (2022). "The REEP family of proteins: Molecular targets and role in pathophysiology." Pharmacol Res **185**: 106477.

Farooqi, I. S., G. S. Yeo, J. M. Keogh, S. Aminian, S. A. Jebb, G. Butler, T. Cheetham and S. O'Rahilly (2000). "Dominant and recessive inheritance of morbid obesity associated with melanocortin 4 receptor deficiency." J Clin Invest **106**(2): 271-279.

Ferre, S. (2015). "The GPCR heterotetramer: challenging classical pharmacology." Trends Pharmacol Sci **36**(3): 145-152.

Grundmann, M. and E. Kostenis (2017). "Temporal Bias: Time-Encoded Dynamic GPCR Signaling." Trends Pharmacol Sci **38**(12): 1110-1124.

Hall, T. A. (1999). "<Bioedit: a user-friendly biological sequence alignment editor and analysis program for Windows 95/98/NT." Nucleic Acids Symposium Series **41**: 3.

Hay, D. L., D. R. Poyner and P. M. Sexton (2006). "GPCR modulation by RAMPs." Pharmacol Ther **109**(1-2): 173-197.

Heroux, M., B. Breton, M. Hogue and M. Bouvier (2007). "Assembly and signaling of CRLR and RAMP1 complexes assessed by BRET." Biochemistry **46**(23): 7022-7033.

Heyder, N., G. Kleinau, M. Szczepek, D. Kwiatkowski, D. Speck, L. Soletto, J. M. Cerda-Reverter, H. Krude, P. Kuhnen, H. Biebermann and P. Scheerer (2019). "Signal Transduction and Pathogenic Modifications at the Melanocortin-4 Receptor: A Structural Perspective." Front Endocrinol (Lausanne) **10**: 515.

Heyder, N. A., G. Kleinau, D. Speck, A. Schmidt, S. Paisdzior, M. Szczepek, B. Bauer, A. Koch, M. Gallandi, D. Kwiatkowski, J. Burger, T. Mielke, A. G. Beck-Sickinger, P. W. Hildebrand, C. M. T. Spahn, D. Hilger, M. Schacherl, H. Biebermann, T. Hilal, P. Kuhnen, B. K. Kobilka and P. Scheerer (2021). "Structures of active melanocortin-4 receptor-Gs-protein complexes with NDP-alpha-MSH and setmelanotide." Cell Res **31**(11): 1176-1189.

Hofland, J., P. J. Delhanty, J. Steenbergen, L. J. Hofland, P. M. van Koetsveld, F. H. van Nederveen, W. W. de Herder, R. A. Feelders and F. H. de Jong (2012). "Melanocortin 2 receptor-associated protein (MRAP) and MRAP2 in human adrenocortical tissues: regulation of expression and association with ACTH responsiveness." J Clin Endocrinol Metab **97**(5): E747-754.

Isbilir, A., J. Moller, M. Arimont, V. Bobkov, C. Perpina-Viciano, C. Hoffmann, A. Inoue, R. Heukers, C. de Graaf, M. J. Smit, P. Annibale and M. J. Lohse (2020). "Advanced fluorescence microscopy reveals disruption of dynamic CXCR4 dimerization by subpocket-specific inverse agonists." Proc Natl Acad Sci U S A **117**(46): 29144-29154.

Isbilir, A., R. Serfling, J. Moller, R. Thomas, C. De Faveri, U. Zabel, M. Scarselli, A. G. Beck-Sickinger, A. Bock, I. Coin, M. J. Lohse and P. Annibale (2021). "Determination of G-protein-coupled receptor oligomerization by molecular brightness analyses in single cells." Nat Protoc **16**(3): 1419-1451.

Janetzko, J., R. Kise, B. Barsi-Rhyne, D. H. Siepe, F. M. Heydenreich, K. Kawakami, M. Masureel, S. Maeda, K. C. Garcia, M. von Zastrow, A. Inoue and B. K. Kobilka (2022). "Membrane phosphoinositides regulate GPCR-beta-arrestin complex assembly and dynamics." Cell **185**(24): 4560-4573 e4519.

Josep Agulleiro, M., R. Cortes, B. Fernandez-Duran, S. Navarro, R. Guillot, E. Meimaridou, A. J. Clark and J. M. Cerda-Reverter (2013). "Melanocortin 4 receptor becomes an ACTH receptor by coexpression of melanocortin receptor accessory protein 2." Mol Endocrinol **27**(11): 1934-1945.

Kay, E. I., R. Botha, J. M. Montgomery and K. G. Mountjoy (2013). "hMRAPa increases alphaMSH-induced hMC1R and hMC3R functional coupling and hMC4R constitutive activity." J Mol Endocrinol **50**(2): 203-215.

Klarenbeek, J., J. Goedhart, A. van Batenburg, D. Groenewald and K. Jalink (2015). "Fourth-generation epac-based FRET sensors for cAMP feature exceptional brightness, photostability and dynamic range: characterization of dedicated sensors for FLIM, for ratiometry and with high affinity." PLoS One **10**(4): e0122513.

Klein, K. R., B. C. Matson and K. M. Caron (2016). "The expanding repertoire of receptor activity modifying protein (RAMP) function." Crit Rev Biochem Mol Biol **51**(1): 65-71.

Kuhnen, P., H. Krude and H. Biebermann (2019). "Melanocortin-4 Receptor Signalling: Importance for Weight Regulation and Obesity Treatment." Trends Mol Med **25**(2): 136-148.

Lattanzi, R., I. Casella, M. R. Fullone, D. Maftei, M. Vincenzi and R. Miele (2024). "MRAP2 Inhibits beta-Arrestin-2 Recruitment to the Prokineticin Receptor 2." Curr Issues Mol Biol **46**(2): 1607-1620.

Li, Y. Q., Y. Shrestha, M. Pandey, M. Chen, A. Kablan, O. Gavrilova, S. Offermanns and L. S. Weinstein (2016). "G(q/11)alpha and G(s)alpha mediate distinct physiological responses to central melanocortins." J Clin Invest **126**(1): 40-49.

Liang, J., L. Li, X. Jin, B. Xu, L. Pi, S. Liu, W. Zhu, C. Zhang, B. Luan, L. Gong and C. Zhang (2018). "Pharmacological effect of human melanocortin-2 receptor accessory protein 2 variants on hypothalamic melanocortin receptors." Endocrine **61**(1): 94-104.

Luo, P., W. Feng, S. Ma, A. Dai, K. Wu, X. Chen, Q. Yuan, X. Cai, D. Yang, M. W. Wang, H. Eric Xu and Y. Jiang (2023). "Structural basis of signaling regulation of the human melanocortin-2 receptor by MRAP1." Cell Res **33**(1): 46-54.

Mainland, J. and H. Matsunami (2012). "RAMP like proteins : RTP and REEP family of proteins." Adv Exp Med Biol **744**: 75-86.

Manglik, A., A. C. Kruse, T. S. Kobilka, F. S. Thian, J. M. Mathiesen, R. K. Sunahara, L. Pardo, W. I. Weis, B. K. Kobilka and S. Granier (2012). "Crystal structure of the micro-opioid receptor bound to a morphinan antagonist." Nature **485**(7398): 321-326.

McLatchie, L. M., N. J. Fraser, M. J. Main, A. Wise, J. Brown, N. Thompson, R. Solari, M. G. Lee and S. M. Foord (1998). "RAMPs regulate the transport and ligand specificity of the calcitonin-receptor-like receptor." Nature **393**(6683): 333-339.

Metherell, L. A., J. P. Chapple, S. Cooray, A. David, C. Becker, F. Ruschendorf, D. Naville, M. Begeot, B. Khoo, P. Nurnberg, A. Huebner, M. E. Cheetham and A. J. Clark (2005). "Mutations in MRAP, encoding a new interacting partner of the ACTH receptor, cause familial glucocorticoid deficiency type 2." Nat Genet **37**(2): 166-170.

Metzger, P. J., A. Zhang, B. A. Carlson, H. Sun, Z. Cui, Y. Li, M. T. Jahnke, D. R. Layton, M. B. Gupta, N. Liu, E. Kostenis, O. Gavrilova, M. Chen and L. S. Weinstein (2024). "A human obesity-associated MC4R mutation with defective Gq/11alpha signaling leads to hyperphagia in mice." J Clin Invest **134**(4).

Moller, T. C., M. F. Pedersen, J. R. van Senten, S. D. Seiersen, J. M. Mathiesen, M. Bouvier and H. Brauner-Osborne (2020). "Dissecting the roles of GRK2 and GRK3 in mu-opioid receptor internalization and beta-arrestin2 recruitment using CRISPR/Cas9-edited HEK293 cells." Sci Rep **10**(1): 17395.

Namkung, Y., C. Le Gouill, V. Lukashova, H. Kobayashi, M. Hogue, E. Khoury, M. Song, M. Bouvier and S. A. Laporte (2016). "Monitoring G protein-coupled receptor and beta-arrestin trafficking in live cells using enhanced bystander BRET." Nat Commun **7**: 12178.

Navarro, G., A. Cordomi, M. Zelman-Femiak, M. Brugarolas, E. Moreno, D. Aguinaga, L. Perez-Benito, A. Cortes, V. Casado, J. Mallol, E. I. Canela, C. Lluis, L. Pardo, A. J. Garcia-Saez, P. J. McCormick and R. Franco (2016). "Quaternary structure of a G-protein-coupled receptor heterotetramer in complex with Gi and Gs." BMC Biol **14**: 26.

Ollmann, M. M., B. D. Wilson, Y. K. Yang, J. A. Kerns, Y. Chen, I. Gantz and G. S. Barsh (1997). "Antagonism of central melanocortin receptors in vitro and in vivo by agouti-related protein." Science **278**(5335): 135-138.

Paradis, J. S., X. Feng, B. Murat, R. E. Jefferson, B. Sokrat, M. Szpakowska, M. Hogue, N. D. Bergkamp, F. M. Heydenreich, M. J. Smit, A. Chevigne, M. Bouvier and P. Barth (2022). "Computationally designed GPCR quaternary structures bias signaling pathway activation." Nat Commun **13**(1): 6826.

Peters, C. H., R. K. Singh, J. R. Bankston and C. Proenza (2022). "Regulation of HCN Channels by Protein Interactions." Front Physiol **13**: 928507.

Piechowski, C. L., A. Rediger, C. Lagemann, J. Muhlhaus, A. Muller, J. Pratzka, P. Tarnow, A. Gruters, H. Krude, G. Kleinau and H. Biebermann (2013). "Inhibition of melanocortin-4 receptor dimerization by substitutions in intracellular loop 2." J Mol Endocrinol **51**(1): 109-118.

Rasmussen, S. G., B. T. DeVree, Y. Zou, A. C. Kruse, K. Y. Chung, T. S. Kobilka, F. S. Thian, P. S. Chae, E. Pardon, D. Calinski, J. M. Mathiesen, S. T. Shah, J. A. Lyons, M. Caffrey, S. H. Gellman, J. Steyaert, G. Skiniotis, W. I. Weis, R. K. Sunahara and B. K. Kobilka (2011). "Crystal structure of the beta2 adrenergic receptor-Gs protein complex." Nature **477**(7366): 549-555.

Reininghaus, N., S. Paisdzior, F. Hopfner, S. Jyrch, C. Cetindag, P. Scheerer, P. Kuhnen and H. Biebermann (2022). "A Setmelanotide-like Effect at MC4R Is Achieved by MC4R Dimer Separation." Biomolecules **12**(8).

Rouault, A. A. J., A. A. Lee and J. A. Sebag (2017). "Regions of MRAP2 required for the inhibition of orexin and prokineticin receptor signaling." Biochim Biophys Acta Mol Cell Res **1864**(12): 2322-2329.

Sawyer, T. K., P. J. Sanfilippo, V. J. Hruby, M. H. Engel, C. B. Heward, J. B. Burnett and M. E. Hadley (1980). "4-Norleucine, 7-D-phenylalanine-alpha-melanocyte-stimulating hormone: a highly potent alpha-melanotropin with ultralong biological activity." Proc Natl Acad Sci U S A **77**(10): 5754-5758.

Scarselli, M., P. Annibale, P. J. McCormick, S. Kolachalam, S. Aringhieri, A. Radenovic, G. U. Corsini and R. Maggio (2016). "Revealing G-protein-coupled receptor oligomerization at the single-molecule level through a nanoscopic lens: methods, dynamics and biological function." FEBS J **283**(7): 1197-1217.

Schonnop, L., G. Kleinau, N. Herrfurth, A. L. Volckmar, C. Cetindag, A. Muller, T. Peters, S. Herpertz, J. Antel, J. Hebebrand, H. Biebermann and A. Hinney (2016). "Decreased melanocortin-4 receptor function conferred by an infrequent variant at the human melanocortin receptor accessory protein 2 gene." Obesity (Silver Spring) **24**(9): 1976-1982.

Sebag, J. A. and P. M. Hinkle (2007). "Melanocortin-2 receptor accessory protein MRAP forms antiparallel homodimers." Proc Natl Acad Sci U S A **104**(51): 20244-20249.

Sebag, J. A. and P. M. Hinkle (2009). "Opposite effects of the melanocortin-2 (MC2) receptor accessory protein MRAP on MC2 and MC5 receptor dimerization and trafficking." J Biol Chem **284**(34): 22641-22648.

Sebag, J. A., C. Zhang, P. M. Hinkle, A. M. Bradshaw and R. D. Cone (2013). "Developmental control of the melanocortin-4 receptor by MRAP2 proteins in zebrafish." Science **341**(6143): 278-281.

Serafin, D. S., N. R. Harris, N. R. Nielsen, D. I. Mackie and K. M. Caron (2020). "Dawn of a New RAMPage." Trends Pharmacol Sci **41**(4): 249-265.

Sharrocks, K. L., F. Fanelli, Y. Lui, A. J. Milner, W. Yining, B. Byrne and A. C. Hanyaloglu (2024).

Soletto, L., S. Hernandez-Balfago, A. Rocha, P. Scheerer, G. Kleinau and J. M. Cerda-Reverter (2019). "Melanocortin Receptor Accessory Protein 2-Induced Adrenocorticotropic Hormone Response of Human Melanocortin 4 Receptor." J Endocr Soc **3**(2): 314-323.

van der Westhuizen, E. T., B. Breton, A. Christopoulos and M. Bouvier (2014). "Quantification of ligand bias for clinically relevant beta2-adrenergic receptor ligands: implications for drug taxonomy." Mol Pharmacol **85**(3): 492-509.

Wade, K. H., B. Y. H. Lam, A. Melvin, W. Pan, L. J. Corbin, D. A. Hughes, K. Rainbow, J. H. Chen, K. Duckett, X. Liu, J. Mokrosinski, A. Morseburg, S. Neaves, A. Williamson, C. Zhang, I. S. Farooqi, G. S. H. Yeo, N. J. Timpson and S. O'Rahilly (2021). "Loss-of-function mutations in the melanocortin 4 receptor in a UK birth cohort." Nat Med **27**(6): 1088-1096.

Wang, M., X. Wang, B. Jiang, Y. Zhai, J. Zheng, L. Yang, X. Tai, Y. Li, S. Fu, J. Xu, X. Lei, Z. Kuang, C. Zhang, X. Bai, M. Li, T. Zan, S. Qu, Q. Li and C. Zhang (2022). "Identification of MRAP protein family as broad-spectrum GPCR modulators." Clin Transl Med **12**(11): e1091.

Webb, T. R. and A. J. Clark (2010). "Minireview: the melanocortin 2 receptor accessory proteins." Mol Endocrinol **24**(3): 475-484.

Weis, W. I. and B. K. Kobilka (2018). "The Molecular Basis of G Protein-Coupled Receptor Activation." Annu Rev Biochem **87**: 897-919.

Wright, S. C., A. Motso, S. Koutsilieri, C. M. Beusch, P. Sabatier, A. Berghella, E. Blondel-Tepaz, K. Mangenot, I. Pittarokoilis, D. C. Sismanoglou, C. Le Gouill, J. V. Olsen, R. A. Zubarev, N. A. Lambert, A. S. Hauser, M. Bouvier and V. M. Lauschke (2023). "GLP-1R signaling neighborhoods associate with the susceptibility to adverse drug reactions of incretin mimetics." Nat Commun **14**(1): 6243.

Wu, B., E. Y. Chien, C. D. Mol, G. Fenalti, W. Liu, V. Katritch, R. Abagyan, A. Brooun, P. Wells, F. C. Bi, D. J. Hamel, P. Kuhn, T. M. Handel, V. Cherezov and R. C. Stevens (2010). "Structures of the CXCR4 chemokine GPCR with small-molecule and cyclic peptide antagonists." Science **330**(6007): 1066-1071.

Zhang, H., L. N. Chen, D. Yang, C. Mao, Q. Shen, W. Feng, D. D. Shen, A. Dai, S. Xie, Y. Zhou, J. Qin, J. P. Sun, D. H. Scharf, T. Hou, T. Zhou, M. W. Wang and Y. Zhang (2021). "Structural insights into ligand recognition and activation of the melanocortin-4 receptor." Cell Res **31**(11): 1163-1175.